Published in final edited form as:
J Neurosci Res. 2007 November 15; 85(15): 3267. doi:10.1002/jnr.21376.

Astrocytic Connexin Distributions and Rapid, Extensive Dye Transfer Via Gap Junctions in the Inferior Colliculus: Implications for [^{14}C]Glucose Metabolite Trafficking

Kelly K. Ball[1], **Gautam K. Gandhi**[2], **Jarrod Thrash**[1], **Nancy F. Cruz**[1], and **Gerald A. Dienel**[1,2,*]

[1]Department of Neurology, University of Arkansas for Medical Sciences, Little Rock, Arkansas

[2]Department of Physiology and Biophysics, University of Arkansas for Medical Sciences, Little Rock, Arkansas

Abstract

The inferior colliculus has the highest rates of blood flow and metabolism in brain, and functional metabolic activity increases markedly in response to acoustic stimulation. However, brain imaging with [1- and 6-^{14}C]glucose greatly underestimates focal metabolic activation that is readily detected with [^{14}C]deoxyglucose, suggesting that labeled glucose metabolites are quickly dispersed and released from highly activated zones of the inferior colliculus. To evaluate the role of coupling of astrocytes via gap junctions in dispersal of molecules within the inferior colliculus, the present study assessed the distribution of connexin (Cx) proteins in the inferior colliculus and spreading of Lucifer yellow from single microinjected astrocytes in slices of adult rat brain. Immunoreactive Cx43, Cx30, and Cx26 were heterogeneously distributed; the patterns for Cx43 and Cx 30 differed and were similar to those of immunoreactive GFAP and S100β, respectively. Most Cx43 was phosphorylated in resting and acoustically stimulated rats. Dye spreading revealed an extensive syncytial network that included thousands of cells and perivasculature endfeet; with 8% Lucifer yellow VS and a 5-min diffusion duration, about 6,100 astrocytes (range 2,068–11,939) were labeled as far as 1–1.5 mm from the injected cell. The relative concentration of Lucifer yellow fell by 50% within 0.3–0.8 mm from the injected cell with a 5-min diffusion interval. Perivascular dye labeling was readily detectable and often exceeded dye levels in nearby neuropil. Thus, astrocytes have the capability to distribute intracellular molecules quickly from activated regions throughout the large, heterogeneous syncytial volume of the inferior colliculus, and rapid trafficking of labeled metabolites would degrade resolution of focal metabolic activation.

Keywords

astrocyte; inferior colliculus; gap junction; Lucifer yellow

In our companion study (Cruz et al., 2007) to the present work, we found that unilateral acoustic stimulation of the conscious rat with a single tone produced tonotopic metabolic activation bands in the inferior colliculus when assayed with [^{14}C]deoxyglucose (DG) but the magnitude of these activation bands was greatly underestimated or not detectable when [1- or 6-^{14}C] glucose was used as the metabolic tracer because of label spreading and loss. Similar findings

*Correspondence to: Gerald A. Dienel, PhD, Department of Neurology, Slot 830, University of Arkansas for Medical Sciences, 4301 W. Markham St., Shorey Bldg., Room 715, Little Rock, AR 72205. gadienel@uams.edu.
The first two authors contributed equally to this work.

of very low registration of brain activation in autoradiographic studies of glucose utilization with increasing duration of the experimental interval (Lear and Ackermann, 1988), during visual stimulation (Collins et al., 1987; Ackermann and Lear, 1989), and during seizures or spreading cortical depression (Ackermann and Lear, 1989; Lear and Ackermann, 1989, 1991; Adachi et al., 1995; Cruz et al., 1999) using [1- or 6-^{14}C]glucose as the tracer indicates rapid loss of labeled metabolites in quantities corresponding to most of the additional glucose consumed during activating conditions. Diffusion of labeled metabolites within the astrocytic syncytium and in extracellular fluid after release from activated cells in the inferior colliculus was implicated as a mechanism for dispersal of glucose metabolites, because label spreading during focal microinfusion of [1-^{14}C]glucose was reduced by prior treatment with gap junction and monocarboxylic acid transporter inhibitors (Cruz et al., 2007). Transfer of [^{14}C]glucose-derived metabolites within the astrocytic syncytium can be mediated by gap junctional channels (Tabernero et al., 1996; Giaume et al., 1997), which are permeable to many small molecules of less than ~1 kDa (Simpson et al., 1977; Loewenstein, 1981), although size and charge of the compound and the connexin protein composition of the channels can influence the extent and direction of movement (Nicholson et al., 2000; Harris, 2001; Nagy and Rash, 2000, 2003; Goldberg et al., 2004; Weber et al., 2004).

The possibility of rapid but selective passage of small molecules through gap junctional channels and regulation of channel permeability by physiological state is of particular interest, because there is substantial local trapping of increased amounts of [^{14}C]DG-6-P but poor retention of products of [1- and 6-^{14}C]glucose in activated cells in the inferior colliculus during acoustic stimulation (Cruz et al., 2007). Focal accumulation of [^{14}C]DG-6-P but not products of [^{14}C]glucose suggests four possibilities: 1) downstream labeled products of [^{14}C]glucose metabolism quickly spread and are released from the activated tissue; 2) the stimulus-induced increase in glucose utilization occurs mainly in cells that are not gap junction coupled (e.g., neurons); 3) astrocytes in the inferior colliculus can contribute to label spreading but are not extensively coupled, so that DG-6-P does not spread very far and tonotopic bands can be imaged; or 4) DG-6-P is not readily transported through gap junction channels. Because gap junctional trafficking could influence results of autoradiographic, positron emission tomographic (PET), and magnetic resonance spectroscopic (MRS) studies of functional metabolism using labeled glucose or its analogs as tracers, the present study evaluated properties of the astrocytic syncytium in the inferior colliculus.

Gap junctional channels contain various connexin (Cx) proteins in different cell types and tissues. Trafficking, assembly, degradation, and gating of channels composed of Cx43, a predominant astrocytic connexin, can be influenced by phosphorylation and dephosphorylation (Lampe and Lau, 2000; Lampe et al., 2000). In normal brain tissue and in gap junction-coupled astrocytes in tissue culture, most of the Cx43 is highly phosphorylated (Hossain et al., 1994; Li et al., 1998; Li and Nagy, 2000a). However, the level of dephosphorylated Cx43 increases under various conditions, e.g., after electrical stimulation of the sciatic nerve (Li and Nagy, 2000b), ischemia (Li et al., 1998), glucose/oxygen deprivation, or treatment of brain slices with 1 mM glutamate or 15 mM K^+ for 1 hr (Nagy and Li, 2000). The relationship between phosphorylation state and gap junctional communication is complex and difficult to evaluate because of changes in epitope recognition (i.e., masking; Nagy and Li, 2000) and various phosphorylation sites that are linked to different signaling pathways that can cause channels to open or close (Lampe and Lau, 2000); few studies have simultaneously examined both phosphorylation status and channel permeability. There is a wealth of evidence that neuronal activity and neurotransmitters and neuromodulators alter gap junctional permeability (Giaume and McCarthy, 1996), e.g., dye transfer is increased by electrical stimulation of frog optic nerve (Marrero and Orkand, 1996) and treatment of cultured astrocytes with glutamate or K^+ (Enkvist and McCarthy, 1994). These and many other studies support the notion that astrocyte-neuron

interactions may act to help synchronize cellular activities within the syncytium via passage of ions, metabolites, and signaling molecules (Bruzzone et al., 1996; Rouach et al., 2004).

In the present study, the capacity of astrocytes in the inferior colliculus to carry out extensive gap junctional trafficking was evaluated by two approaches. First, the relative abundance and distributions of three astrocytic connexin proteins (Cx43, Cx30, and Cx26) and the overall phosphorylation state of Cx43 during rest and acoustic stimulation were assessed via immunohistochemical methods. Then, fluorescent dye transfer after microinjection of Lucifer yellow (LY) into single astrocytes in slices of inferior colliculus was used to evaluate syncytial size and the extent of gap junction-mediated transfer of small molecules. Because microinjection was carried out under visual direction, it was first necessary to establish the distributions of astrocyte marker proteins in the inferior colliculus and their stability in tissue slice preparations so that they could be appropriately used as markers for dye colocalization. The results demonstrate that the inferior colliculus has abundant quantities of connexins with differential distributions and a large, rapidly labeled astrocytic syncytium.

MATERIALS AND METHODS

Materials

Phosphate-buffered 10% formalin, pH 6.9–7.1, was purchased from Poly Scientific R&D Corp. (Bay Shore, NY). Superfrost/Plus microscope slides, Permount, Gill's No. 3 Hematoxylin Solution, and eosin Y were obtained from Fisher Scientific (Pittsburgh, PA). Halothane was purchased from Halocarbon Laboratories (Riveredge, NJ). Reagents for immunolabeling assays were from the following sources: rabbit anti-cow glial fibrillary acidic protein (GFAP), rabbit anti-human S100β; swine and goat serum, swine anti-rabbit IgG, rabbit peroxidase antiperoxidase (PAP; Dako, Carpinteria, CA); rabbit polyclonal anti-Cx43 (H-150), goat polyclonal anti-Cx43 (C-20 or sc-6560), and anti-Cx43 blocking peptide (sc-6560p; Santa Cruz Biotechnology, Santa Cruz, CA); rabbit polyclonal anti-Cx30, rabbit polyclonal anti-Cx26, rabbit anti-Cx43, goat anti-rabbit IgG, and control peptide for Cx43 (Zymed, South San Francisco, CA); mouse monoclonal anti-MAP2 (2a + 2b) clone AP-20, alkaline phosphatase, sodium vanadate, sodium fluoride, dibutyryl cyclic adenosine monophosphate, L-leucine methyl ester hydrochloride, octanol, Lucifer yellow CH and Lucifer yellow VS (both dilithium salts), Triton X-100, and Sigma Fast DAB Peroxidase Substrate Tablet Set (Sigma, St. Louis, MO); Texas red-X goat anti-rabbit IgG, Alexa Fluor 350 goat anti-rabbit IgG, and Alexa Fluor 488 donkey anti-goat IgG (Molecular Probes, Eugene, OR); donkey serum and Gelmount medium (Biomeda Corp., Foster City, CA); molecular weight standards and Bradford protein assay reagent (Bio-Rad, Hercules, CA); T-PER tissue protein extraction reagent (Pierce, Rockford, IL); Hybond ECL nitrocellulose membranes and ECL Plus Western blotting reagent pack (GE Healthcare, Piscataway, NJ); Complete Protease Inhibitor Cocktail Tabs (Roche, Indianapolis, IN); Dulbecco's modified Eagle's medium (Catalog No. 12320-032), penicillin, streptomycin, and trypsin (Invitrogen; Carlsbad, CA); and fetal bovine serum (Hyclone, Logan, UT). Pregnant females and male albino Wistar rats (250–350g) were purchased from Taconic (Germantown, NY). All animal use procedures were in strict accordance with the NIH *Guide for care and use of laboratory animals* and were reviewed and approved by the local animal care and use committee.

Immunohistochemical Procedures

Perfusion Fixation—Nine rats were deeply anesthetized with pentobarbital and perfusion fixed according to the procedure of Yamamoto et al. (1990a,b, 1992). In brief, rats were first perfused transcardially with an ice-cold (4°C) wash solution containing 50 mM sodium phosphate buffer (PB), pH 7.8, 0.9% saline, 0.1% sodium nitrite, and 1 U/ml heparin. When the wash effluent was clear of blood, rats were perfused with cold 4% paraformaldehyde in

0.1 M PB, pH 7.4, for 10 min, followed by cold 4% paraformaldehyde in 50 mM sodium borate buffer, pH 9.0, for 10 min. Brains were dissected out, postfixed overnight at 4°C in 4% paraformaldehyde containing 50 mM sodium borate, pH 9.0, then submerged in 10% sucrose in 50 mM PB, pH 7.4, for 4–5 hr, transferred to 30% sucrose in 50 mM PB, pH 7.4, and stored at 4°C overnight. On the next day, the brains were frozen in isopentane cooled to −;45°C on dry ice and stored at −80°C. Prior to sectioning in a Leica CM 1850 cryostat (Leica Microsystems, Wetzlar, Germany), brains were warmed to −20°C for 2 hr, then cut into 40-μm-thick sections. Coronal sections were prepared from eight brains, and sagittal sections were made from one brain. The free-floating sections were stored overnight in multiwell tissue culture plates in PTX (0.1 M phosphate buffer containing 0.9% saline, pH 7.4 [PBS], containing 0.3% Triton X-100). PAP (Sternberger, 1979) and immunofluorescence methods of immunohistochemistry were used to assess the distributions of immunoreactive Cx43, Cx30, and Cx26, GFAP-positive cells and S100β-positive cells, as described below.

PAP Staining Procedure—Sections were rinsed three times for 5 min/wash in PTX, and endogenous peroxidases were blocked by a 15-min incubation in 50% methanol, 50% PTX, plus 0.3% hydrogen peroxide, followed by two 5-min washes in PTX and a 30-min incubation in blocking solution (10% swine serum in PTX). The sections were then incubated for 48 hr at 4°C with one of five primary antibodies that were diluted in PTX with 10% normal swine serum: rabbit polyclonal anti-Cx43 (H-150) diluted 1:50, rabbit polyclonal anti-Cx30 (1:200), rabbit polyclonal anti-Cx26 (1:50), rabbit anti-cow GFAP (1:1,000), or rabbit anti-human S100β (1:1,000). Control sections were treated identically except that the primary antibody was omitted. The sections were then washed three times in PTX, incubated with the secondary antibody, swine anti-rabbit IgG diluted 1:500 in 10% swine serum PTX for 1 hr, followed by three more 5-min washes with PTX. After washing, sections were transferred to a solution of rabbit PAP (diluted 1:100 in PB) for a minimum of 45 min and then given three 5-min PTX washes, followed by incubation in the dark for 8–10 min in a 3,3′-diaminobenzidine (DAB) solution using the Sigma Fast DAB Peroxidase Substrate Tablet Set prepared according to the manufacturer's instructions. Next, sections were rinsed twice in PBS and once in deionized H_2O, mounted onto Superfrost/Plus microscope slides, and air dried overnight at room temperature. Slides were either passed through xylene and coverslipped with Permount histological mounting medium or stained with Gill's No. 3 Hematoxylin Solution and eosin Y, passed through graded alcohols and xylene, and coverslipped.

Immunofluorescence Procedure—Sections were washed three times in PTX, blocked by a 30-min incubation in 10% goat serum in PTX, and incubated for 48 hr in primary antibody at 4°C; the same primary antibodies were used at the same dilutions as described above, except the diluent was 10% goat serum-PTX. In addition, mouse monoclonal anti-MAP2 (2a + 2b) clone AP-20 diluted 1:1,000 (and incubated for 24 hr) was employed as a neuronal marker. Control slides were treated identically except that the primary antibody was omitted. Goat polyclonal anti-Cx43 (C-20) was also used as a primary antibody because a blocking peptide was available for use as a second control for nonspecific binding. After the initial three 5-min PTX washes and preincubation in 10% donkey serum-PTX for 30 min, sections were incubated in anti-Cx43 (C-20) primary for 48 hr at 4°C, using a 1:50 dilution in 10% donkey serum PTX. For control assays, anti-Cx43 (C-20) was first preabsorbed with five times the amount of blocking peptide in a small volume of PBS for 2 hr at room temperature, brought to the appropriate dilution with 10% donkey serum PTX, and sections were incubated for 48 hr at 4° C. All experimental and control tissue sections were given three 5-min washes, followed by incubation for 1 hr with one of the following: Texas red-X goat anti-rabbit IgG, Alexa Fluor 350 goat anti-rabbit IgG, Texas red goat anti-mouse IgG, or Alexa Fluor 488 donkey anti-goat IgG diluted 1:500 in 10% serum PTX, using the appropriate serum and secondary antibody for each assay. Then, the sections were washed three more times for 5 min each, rinsed in deionized

H_2O, placed on microscope slides, and mounted in Gelmount. Tissue sections were examined with a Zeiss Axioskop 2 microscope, black-and-white images were captured with a MTI CCD 72 camera (Dage-MTI, Michigan City, IN) and processed with MCID Imaging Software (Imaging Research, St. Catharines, Ontario, Canada).

Gel Electrophoresis and Western Blotting

Tissue from different brain regions from a separate group of 23 rats was obtained by dissection of tissue that was obtained by decapitation or in situ freezing (see below) during "resting," unstimulated conditions or after 15 or 45 min of broadband click tone acoustic stimulation (40 Hz to 8 kHz, 103 dB) to activate neural activity in the auditory pathway (Grass Instruments Click-Tone Module and Audiometric Headphones; for details see Cruz et al., 2007). One group of rats was briefly anesthetized with pentobarbital given intravenously and immediately decapitated; regions of interest were quickly dissected out of the chilled brain and frozen in isopentane at about −45°C within 2–4 min after decapitation. Alternatively, brains of a second group of rats briefly anesthetized with intravenous thiopental were immediately "funnel-frozen" in situ with liquid nitrogen, and then regions of interest were dissected out and weighed in a cryobox at −25°C, as previously described in detail (Cruz and Dienel, 2002; Dienel et al., 2002). All tissue samples were stored at −80°C until homogenization with a Brinkman Polytron in T-PER extraction buffer containing Complete Protease Inhibitor Cocktail plus two phosphatase inhibitors, sodium fluoride (10 mM) and sodium vanadate (1 mM). The homogenates were centrifuged and supernatant fractions assayed for protein contents by using the Bradford assay and bovine serum albumin as the standard. Tissue samples (2.5–10 μg protein/lane) and molecular weight standards were separated on one-dimensional sodium dodecyl sulfate (SDS)-polyacrylamide gels (4% stacking gel, 10% separating gel), proteins were electrophoretically transferred to nitrocellulose membranes that were then washed, equilibrated in Tris-buffered saline, pH 7.5, blocked (incubated in 5% Carnation instant dry milk and 0.1% Tween 20 in Tris-buffered saline, pH 7.5, for 2 hr at 4°C, with gentle shaking), incubated with the Zymed Cx43 antibody (1:10,000 or 1:20,000 dilution in Tris-buffered saline containing 0.1% Tween 20 for 2 hr or overnight at 4°C, with gentle shaking), washed (four times with changes of Tris-buffered saline containing 0.1% Tween 20: once for 5 min, once for 15 min, twice for 5 min), incubated with the Zymed secondary antibody (1:10,000 or 1:20,000 dilution for 1 hr at 4°C, with gentle shaking) and washed four times as described above. Then, the membranes were incubated in ECL Plus reagents according to manufacturer's instructions, exposed to X-ray film, and analyzed with a Molecular Dynamics Phosphor-Imager. For negative control experiments, the Zymed Cx43 primary antibody was preincubated with the Zymed Cx43 blocking peptide prior to incubation with nitrocellulose membranes. To verify that isoforms of Cx43 are phosphorylated, solublized fractions of tissue extracts (300 μg protein) were incubated with alkaline phosphatase (70–100 units) for 3 hr at 37°C in 100 mM Tris, pH 8.0, after preincubation of enzyme for 30 min at 37°C in the presence or absence of phosphatase inhibitors (10 mM NaF plus 1 mM Na_3VO_4).

Brain Slice Preparation

Brain slices were prepared from separate groups of rats to 1) assess immunohistochemical staining of routinely used cell-type markers (GFAP, S100β, and MAP2) with time after slice preparation using minor modifications of established procedures (Ludwin et al., 1976; Inagaki et al., 1997) and 2) evaluate properties of the astrocyte syncytium after microinjection of various concentrations of fluorescent dye into a single astrocyte in a slice in the inferior colliculus. Rats were deeply anesthetized with halothane and decapitated; brains were rapidly removed, immediately chilled by immersion in oxygenated, ice-cold artificial cerebral spinal fluid solution containing 26 mM $NaHCO_3$ (pH 7.3) and 248 mM sucrose, and 250-μm-thick coronal slices of midbrain that includes the inferior colliculus were cut with a Leica VT 1000S vibrating blade microtome. For post-mortem recovery, the slices were incubated in oxygenated

artificial cerebral spinal fluid containing 248 mM sucrose for 30 min at 35°C, then at 22°C for at least 1 hr (Moyer and Brown, 1998), and transferred to a Series 20 perfusion chamber (Warner Instruments, Hamden, CT) for microinjection studies (see below).

Gap Junction-Mediated Dye Transfer Assays

Borosilicate glass (1 mm OD, 0.5 mm ID) micropipettes (12–14 MO; Flaming/Brown P97 pipette puller; Sutter Instruments, Novato, CA) were filled with solutions containing (composition in mM) 21.4 KCl, 0.5 $CaCl_2$, 2 $MgCl_2$, 5 EGTA, 2 ATP, 0.5 GTP, 2 ascorbate, 10 HEPES, pH 7.2, and fluorescent tracers. The molecular weight and cellular labeling properties of LY dyes (excitation/emission maxima: 430/530 nm) differ (Stewart, 1981); LYVS (536 Da when ionized) labels prominantly nuclei (Enkvist and McCarthy, 1992, 1994), whereas LYCH (443 Da when ionized) has a greater cytoplasmic than nuclear distribution. The final concentrations of the fluorescent probes in the pipette solution were 8% LYVS (124 mM) or 2% or 4% LYVS plus 2% or 4% LYCH. The osmolarity of each solution was measured (Osmette II, Precision Systems, Natick MA) and adjusted to 305–320 mOsm with sucrose.

Slices of inferior colliculus from adult male rat brain were transferred to the microscope stage and perfused (1 ml/min) with ACSF containing 26 mM $NaHCO_3$ (pH 7.3) and 10 mM glucose. The perfusion solution was freshly prepared, kept at room temperature, and continuously bubbled with oxygen/CO_2 (95/5%). Astrocytes in brain slices were visualized via infrared-differential interference contrast (IR-DIC) with a Nikon Eclipse E600 microscope (Melville, NY) using a Photometrics CoolSNAP ES camera (Roper Scientific, Atlanta, GA) and MetaVue software (Molecular Devices, Sunnyvale, CA). Under visual direction, astrocytes were impaled with micropipettes using a MP-225 manipulator (Sutter Instruments, San Francisco, CA), and the LY solutions were allowed to diffuse into the cell for 5 min. Then, each slice was immediately immersed in and mixed with 10 ml of freshly prepared 4% paraformaldehyde in 0.1 M phosphate-buffered saline, pH 7.4, on a platform shaker for 1 hr at room temperature, then stored at 4°C for 24 hr. Immediate fixation plus mixing was essential for retention of the LY in the slice. In preliminary experiments, use of lower fixative concentrations or failure to mix the immersed slice quickly in fixative resulted in loss of most or all of the LY from slices that were previously extensively labeled; similar losses during fixation occur in retinal preparations (Zahs and Wu, 2001). To assess stability of cell-type markers to this in vitro slice incubation protocol, which is necessary for post-mortem recovery (Moyer and Brown, 1998), one set of slices was immediately immersion fixed after the slices were cut, kept in fixative for 24 hr, then immersed in 30% sucrose solution overnight; a second group was immersion fixed after ~3.5 hr in the 22°C bath (4 hr post-mortem).

Each of the 250-μm-thick fixed slices was cut into 20-μm-thick serial sections, and the number of labeled cells in each section was counted as visible nuclei, with care to avoid replicate counts of nuclei in serial sections. Then, each section was imaged for the following determinations made in Meta-Vue software: 1) the distance from the most highly fluorescent cells at the injection site to the farthest visible cell was measured, 2) the tissue area containing the LY-labeled cells determined by drawing a line along the outer boundary that surrounds and contains the dye-labeled cells (this approach determined the area of tissue within which a labeled syncytium was located, not the areas of individual dye-labeled cells), and 3) the total area of the ipsilateral inferior colliculus determined by outlining the entire inferior colliculus. Volumes for tissue containing the labeled syncytia and the entire inferior colliculus in each 250-μm-thick slice were calculated as the sum of the volumes calculated for each 20-μm-thick section [area in mm^2 × thickness (0.02 mm)]. Because some loss of fluorescent dye during brain tissue fixation is anticipated and cell counts are likely to be underestimated as a result of conservative counting of nuclei, the reported values are considered to be minimal. After labeling with the

LYVS-CH mixture and fixation, selected brain slices were cut into 7-μm-thick serial sections, immunostained, imaged, and analyzed for colocalization of LY and cell-type markers with a Nikon E600 microscope and MetaVue software.

RESULTS

Heterogeneous Distribution of Astrocytic Markers and Connexins in the Inferior Colliculus

Astrocyte Identification—Astrocytes were microinjected by visual guidance when gap junction-mediated dye transfer was assessed in slices of the inferior colliculus, and it was, therefore, necessary to establish the distribution of cell-type markers throughout the inferior colliculus prior to their use to verify the identity of dye-labeled cells. When the distributions of immunoreactive GFAP and S100β, two commonly used markers for astrocytes (Ludwin et al., 1976), were assessed in perfusion-fixed brain in situ and at intervals after slice preparation, substantial differences were observed for major brain structures as well as within subregions of the inferior colliculus. For example, the level of GFAP-immunoreactive protein is much lower in inferior and superior colliculus compared with cerebral cortex, molecular layer of the cerebellum, and hippocampus (Fig. 1A). More GFAP-positive cells and finer cellular details were visualized by immunofluorescence compared with the PAP method because of lower background, but both procedures label far fewer GFAP-positive cells in the interior of the inferior colliculus than in the perimeter; these cells appear highly localized around blood vessels (Fig. 1B–D; see also Fig. 7). Highest labeling of GFAP-positive cells in the inferior colliculus is in the meninges and adjacent tissue (Fig. 1B) as well as in the cells immediately adjacent to and surrounding the aqueduct (Fig. 1C), which is consistent with findings of Hafidi and Galifianakis (2003) in the adult gerbil. In contrast to GFAP, S100•-positive cells were more uniformly present throughout the superior and inferior colliculus, cerebral cortex, hippocampus, and molecular layer of cerebellum (Fig. 1E; compare with cell density stains in Fig. 1K). Immunoreactive S100β is densely distributed throughout the inferior colliculus, with highest labeling in meninges and around the aqueduct (Fig. 1E–H) and a tendency for moderately higher staining in the central zone of the inferior colliculus (Fig. 1G); also, nuclei are more highly labeled compared with cytoplasm (Fig. 1E–H; Ludwin et al., 1976; Cocchia, 1981). As shown by H&E staining, the cell density of the inferior colliculus is high (Fig. 1K,L), contrasting with the cerebral cortex (not shown). By use of fluorescent secondary antibodies, immunoreactive GFAP and S100β were colocalized in structures along blood vessels and in cells surrounding the aqueduct (not shown); both are low in white matter (Fig. 1A,E,J). Omission of the primary antibody gave low nonspecific binding (Fig. 1I). Because immunodetection of these cell-type-marker proteins varies regionally within the brain and also in the inferior colliculus, inclusion or exclusion of cells of interest as astrocytes on the basis of immunohistochemical staining must be made with care.

The above-mentioned cautionary note also extends to immunohistochemical identification of astrocytes in brain slices after intracellular microinjection or electrophysiological studies. Immunoreactive GFAP was robust in slices that were fixed immediately after cutting, with detailed preservation of astrocytic processes (Fig. 2A), whereas, after an ~4-hr incubation in the routinely used brain slice recovery solutions, GFAP immunostaining in the inferior colliculus was, in general, very poor, with fragmentary staining and loss of fine processes (Fig. 2D). Curiously, astrocytes in structures ventral to the inferior colliculus did retain their fibrous structure when stained after in vitro incubation (not shown), suggesting regional sensitivity to post-mortem changes in GFAP immunoreactivity. On the other hand, immunohistochemical staining by anti-S100β was equivalent after immediate or delayed fixation (Fig. 2B,E), and similar findings were obtained for a neuronal marker (Inagaki et al., 1997) using anti-MAP2 (Fig. 2C,F). Thus, S100β is a better marker than GFAP for identifying astrocytes in inferior

colliculus slices and S100β and MAP2 were, therefore, used to evaluate localization of LY after microinjection of single cells.

Cx43, Cx30, and Cx26 Distributions in the Inferior Colliculus of Adult Rats— Cx43, Cx30, and Cx26 are all present in the inferior colliculus but with different localization patterns when visualized with the chromogen DAB (Fig. 3). Immunoreactive Cx43 revealed light, punctate staining throughout the entire inferior colliculus in all eight animals studied, with heaviest staining in meninges, in cells around the aqueduct, and along blood vessels, as illustrated in representative coronal sections (Fig. 3A,B). More Cx43 could be detected in the interior of the inferior colliculus with immunofluorescence (not shown) than with DAB, but the patterns were similar with both procedures and resembled that of GFAP (compare Figs. 1 and 3). By visual inspection, immunoreactive Cx30 was also extensively distributed throughout the inferior colliculus but was more uniformly distributed than Cx43, with somewhat heavier labeling of larger, punctate structures in the central nucleus of the inferior colliculus, a distribution pattern more similar to that of S100β than to that of GFAP (Figs. 1, 3). Both Cx43 and Cx30 were evident along blood vessels in the inferior colliculus (Fig. 3B,F), exhibiting a punctate, honeycomb pattern typical of that reported in other brain structures (see also Fig. 7), which represents gap junctions between apposing astrocytic endfeet (Yamamoto et al., 1990a,b;Nagy et al., 1999). Detection of immunoreactive Cx43 was quite sensitive to the preparative perfusion procedure, and reproducible results with consistent, low background staining levels were obtained only by using the procedure described by Yamamoto et al. (1990a,b,1992). Immunoreactive Cx26 was very weak within the neuropil of inferior and superior colliculus (Fig. 3I–K) and cerebral cortex (not shown) but was higher in the meninges and in cells around the aqueduct (Fig. 3I,K); this differential staining is more evident with use of a fluorescent secondary antibody (Fig. 3J). Notably, immunoreactive Cx30 was readily detectable in tissue prepared by all procedures. Omission of primary antibodies gave very weak background staining (Fig. 3C,D,G,H,L).

The phosphorylation state of Cx43 was assessed during rest and acoustic stimulation of conscious rats, because Cx43 can be dephosphorylated under activating conditions, potentially altering gap junctional coupling (see the introductory paragraphs). Similar Cx43 isoform patterns were observed on Western blots from seven brain regions obtained during “resting” conditions, with most of the immunoreactive protein recovered in the P2 band with higher apparent molecular weight (Fig. 4A). Acoustic stimulation for 15 or 45 min did not alter the overall phosphorylation state in the inferior colliculus compared with the resting state with ambient laboratory noise levels; the relative isoform abundance, P2 > P1 > NP, was evident in all samples prepared by different procedures designed to rule out the possibility of post-mortem changes (Fig. 4B). Pretreatment of tissue extracts with alkaline phosphatase eliminated the more slowly migrating bands (P1 and P2), confirming the phosphorylation status of these isoforms (Fig. 4C). To summarize, most Cx43 is highly phosphorylated in vivo and is not altered by functional activation of the auditory pathway.

Dye Transfer Assays of Astrocytic Gap Junction Coupling in the Inferior Colliculus In Situ

Apparent Syncytial Size—Tonotopic metabolic activation bands resulting from focal trapping of [^{14}C]deoxyglucose-6-phosphate (DG-6-P) were readily detected during 5- or 30-min experimental intervals during monotonic 8-kHz acoustic stimulation of conscious rats (Fig. 5A), but detection of functional activation with [1- or 6-^{14}C]glucose was blunted, in part because of spreading and release of labeled metabolites of glucose by routes that include monocarboxylic acid transporter-and gap junction-mediated trafficking (Cruz et al., 2007). The number and distribution of gap junction-coupled astrocytes in inferior colliculus were, therefore, evaluated by fluorescent dye spreading assays using LY, a membrane-impermeant anionic compound. After visually guided microinjection of a single astrocyte located near the

site of the tonotopic bands (Fig. 5B), the dye was allowed to diffuse from the pipette for 5 min, a labeling interval equal to the duration of [^{14}C]glucose labeling experiments (Cruz et al., 2007). Initial experiments used a mixture of 4% LYVS + 4% LYCH and revealed thousands of dye-labeled astrocytes at distances as far as 1.3 mm from the injected cell (Fig. 5B,Table I). The number of labeled cells averaged about 2,200 within 5 min with this injection protocol, but cellular labeling was quite variable from slice to slice (Table I). Because our preliminary experiments indicated that the number of dye-coupled cells could be greatly underestimated because of incomplete fixation of LY (see Materials and Methods), various mixtures were assessed to evaluate sensitivity of labeling to dye concentration. The mean number of labeled cells rose 7-fold, from 321 to 2,204, when the pipette dye concentration was doubled from 2% LYVS + 2% LYCH to 4% LYVS + 4% LYCH, and, unexpectedly, labeling rose another 2.8-fold to 6,100 when 8% LYVS was the labeling reagent; pretreatment of slices with octanol to block gap junctions reduced dye transfer by >99% (Table I). A striking difference between astrocyte labeling by LYVS or LYCH (Stewart, 1981) is that LYVS is preferentially concentrated in nuclei (Enkvist and McCarthy 1992,1994), with weaker labeling of astrocytic soma, fine processes, and perivascular endfeet; this feature simplifies cell counts because of a higher signal-to-noise ratio in the nuclei. In contrast, LYCH is more highly dispersed throughout the astrocytes, facilitating visualization of the entire intracellular volume and perivascular labeling of blood vessels, with the disadvantage that there is a stronger background "haze" in the neuropil (Fig. 5C); it is, therefore, more difficult to distinguish and count individual labeled cells with LYCH compared with LYVS as the sole labeling reagent.

The pattern of labeled cells often exhibited a tendency for a radially directed distribution of highly fluorescent cells from the injection site toward the periphery of the inferior colliculus (Fig. 5B) rather than a more concentric distribution around the injected cell, as reported for hippocampus (Konietzko and Müller, 1994) and visual cortex (Binmöller and Müller, 1992), although there was some label spread in all directions. Notably, many injected tissue sections showed high labeling along the rim of the inferior colliculus compared with nearby neuropil (inset, Fig. 5B), suggesting a diffusion barrier near the boundary of the inferior colliculus with the meninges (which was removed prior to tissue slicing) that led to dye accumulation. The tissue volume containing a syncytium linked to the single-injected astrocyte was almost 1% of the volume of the ipsilateral inferior colliculus in a 250-μm-thick slice (Table I). The LY-labeled cells were identified as astrocytes on the basis of colocalization with an astrocytic marker, S100β (Fig. 5C–E), and not with a neuronal marker, MAP2 (Fig. 5F–H). Overall, 97% of 278 LY-labeled cells colocalized with S100β, whereas dye labeling of MAP2-positive cells was negligible (Table I). Thus, the astrocytes in the inferior colliculus are highly interconnected, involving thousands of cells located in a nonuniform distribution pattern throughout the tissue (Fig. 5, Table I). To summarize, the magnitude of gap junction coupling of astrocytes in the inferior colliculus is much higher than previously reported in other brain regions, but the true extent is anticipated to be even greater than that observed in the present study because of underestimates arising from technical issues, including the use of a short 5-min labeling period, incomplete dye fixation, and use of a relative large dye tracer (see Discussion).

Extent of Dye Transfer—Counts of dye-coupled cells identify syncytial size and heterogeneous connectivity but do not provide information about the quantity of material transferred from the injected cell to other coupled cells. To estimate the extent of equilibration of dye concentration in recipient astrocytes with that in cells near the injection site within a 5-min interval, the fluorescence intensity of individual labeled astrocytes was determined in groups of cells located at various distances from the point source (Fig. 6). The representative montage illustrates the locations of four sites (300 × 300 μm boxes) in which the relative fluorescence intensity of cells was measured, one box surrounding the injected cell, one about half the distance from the injection site to a third site near the tissue boundary, and a control

region that was poorly labeled (Fig. 6A). As expected from diffusion down a concentration gradient, the average LY fluorescence intensity of labeled astrocytes fell with distance, and, in a representative slice, the levels were 55% and 43% that of the injection site at 670 and 1,370 μm, respectively (Fig. 6B). Even at the tissue boundary site, the average intensity of dye-labeled cells was three times the background fluorescence (Fig. 6A,B); this background arises, in large part, from paraformaldehyde fixation of tissue. On the basis of similar analysis of four slices, the estimated distance at which LY level fell by 50% was 0.79 mm from the injection site (Fig. 6C); conceivably, there could be fluorescence quench in the most highly labeled cells, and, if the LY fluorescence near the injection site were underestimated by a factor of two because of quench, the calculated distance Cx/Co = 0.5 would be 0.34 mm (see legend to Fig. 6). Thus, within 5 min, astrocytes located within the range 0.3–0.8 mm from a point source can attain an estimated concentration of about half that of the source, and dispersal of gap junction-permeable compounds among thousands of astrocytes can be quantitatively substantial.

Astrocytic endfeet are linked together by gap junctions (Yamamoto et al., 1990a,b) and, after injection into a cerebral cortical astrocyte, LY can be transferred along an immediately adjacent vessel via endfeet (Simard et al., 2003). In the inferior colliculus, astrocytic processes that link the soma to endfeet surrounding blood vessels are readily visualized by immunoreactive GFAP (Fig. 7A,B), and punctate endfoot structures are enriched with immunoreactive Cx43 (Fig. 7C) and Cx30 (Fig. 7D). At 5 min after injection of LY into a single astrocyte near the center of the inferior colliculus, the perivascular compartment is highly labeled throughout the large dye-demarcated syncytium as far as 1 mm or more from the injected cell, not just around the injection site (Fig. 7E–I). Highly fluorescent LY-labeled cell bodies are visible in Figure 7E, and one dye-labeled cell has a process that extends close to a blood vessel that is clearly outlined by dye labeling, as is a second, larger vessel (Fig. 7E, dotted arrows). Perivascular endfoot fluorescence clearly demarcates the unlabeled lumen in cross-sections of single vessels (Fig. 7F,G). The relative fluorescence intensity surrounding various vessels was heterogeneous and often higher than that in adjacent neuropil (Figs. 7F–H), identifying coupled endfeet as a prominent dye transfer route. Line-scan analysis of fluorescence intensity (Fig. 7I) along the wall of a long section of a highly labeled vessel compared with nearby tissue (Fig. 7H) shows that the perivascular dye content decreased with distance from left to right. Segments of vessel surround had dye levels twice as high as the level in parenchyma and 50% greater than the level in astrocytic cell bodies that registered as “spikes” in the tissue line scan (Fig. 7I). Similar results (not shown; see legend to Fig. 7) were obtained for perivascular regions of seven additional vessels located 0.6–1.2 mm from the injection site. Thus, routes for dispersal of material from a single dye-injected astrocyte involve not only the astrocytic soma, nucleus, and large and small processes but also gap junction-coupled endfeet that surround the vasculature.

DISCUSSION

Astrocytic Coupling in the Inferior Colliculus

The inferior colliculus has the highest rates of blood flow and glucose utilization in brain (Sokoloff et al., 1977; Gross et al., 1986, 1987) to provide the necessary quantities of nutrients for transfer across vascular and cellular membranes and generate the energy required for acoustic information processing. Functional activation increases glucose utilization in the inferior colliculus, which can be readily imaged with [^{14}C]DG but not [1- or 6-^{14}C]glucose. The present study focuses on 1) the relative abundance and distribution of astrocytic connexins within the inferior colliculus and associated meninges and 2) dye dispersion from a point source to other cells within astrocytic syncytia of the inferior colliculus. These findings help evaluate the potential contributions of gap junction-mediated metabolite trafficking to poor registration of tonotopic bands by [^{14}C]glucose (Cruz et al., 2007) and the likelihood of lactate dispersion

and release during brain activation (Dienel and Cruz, 2004, 2006). Taken together, our major findings demonstrate that immunoreactive Cx43 and Cx30 are abundant in the astrocytes and their perivasculature structures as well as being present at much higher levels, along with Cx26, in the meninges and cells around the aqueduct (Figs. 3, 7). Even with a brief, 5-min diffusion interval, a single astrocyte is linked to many thousands of others via gap junctions to form an extensive syncytial network (Table I, Figs. 5–7) that may be connected to the meningial system (Mercier and Hatton, 2000). This network extends as far as 1.5 mm from the injected cell, ranging from the center of the inferior colliculus to the meninges at the tissue boundary; it is contained within a tissue volume equivalent to about 1% of the volume of the inferior colliculus in the brain slice. Gap junction-mediated diffusion facilitates rapid transfer of material throughout the soma, processes, and perivascular endfeet of interconnected astrocytes, and recipient cells located 0.3–0.8 mm away from a single donor cell can achieve a dye concentration approaching half that in the donor within 5 min. Gap junction channels are known to be permeable to many ions and compounds that enter and leave cells via membrane transporters (e.g., potassium, amino acids, glucose, and lactate) as well as numerous metabolites and signaling compounds restricted to intracellular fluid by lack of transporters or from phosphorylation or other metabolic transformations that render them membrane impermeant. Transfer of LY, a membrane-impermeant dye, represents the latter category, and smaller biological compounds would be expected to diffuse more extensively, depending on their metabolic fate in recipient cells. Extensive dye spreading strongly supports our working hypothesis that labeled metabolites of glucose are quickly dispersed and ultimately released from activated cells, in part, by diffusion through gap junctions (Dienel and Cruz, 2004, 2006), which may facilitate clearance via a larger cellular volume and surface area involving the vascular, meningial, and ventricular systems.

Methodological Issues That Influence Evaluation of Astrocytic Coupling

Assays of gap junctional transfer of biological molecules are difficult because of the lack of sensitive, specific, real-time assays, and fluorescent dyes are, therefore, frequently used as surrogates to evaluate cell—cell coupling. This analysis requires demonstration of coregistration with cell-type markers, with special attention to the technical procedures required to avoid potential pitfalls, including poor dye fixation, differential vulnerability of astrocytic markers to assay conditions, connexin sensitivity to preparative procedures, and regional variations in GFAP-, S100β-, and Cx-immunoreactive protein levels. Wide variability among the reported extent of astrocytic coupling in the central nervous system arises from both technical and biological factors that influence detection and extent of gap junctional transfer, including the duration and mode of delivery of test compounds (micropipette size, diffusion, pressure ejection, iontophoresis), properties of the tracer (size, charge, shape, concentration, binding to cellular constituents, sensitivity for detection), Cx composition of coupled cells, and brain region. For example, in retina, 2–9 mM LYCH (443 Da) labeled two to 10 astrocytes but no Müller cells after 5 min of diffusion from patch pipettes, whereas concomitant labeling by 11 mM neurobiotin (288 Da) contained in the same pipette labeled 13–88 astrocytes plus 118–288 Müller cells (Zahs and Newman, 1997). In hippocampus, regional differences in syncytial size are evident in the CA1 and CA3 hippocampus; up to a few hundred cells were labeled by 0.5% biocytin (372 Da) during patch clamp studies (D'Ambrosio et al., 1998; Theis et al., 2003) and high labeling densities (12–43,000 cells/mm^2) with a general circular pattern around the infused cell resulted from iontophoresis of 5% neurobiotin for 1 hr using sharp pipettes (Konietzko and Müller, 1994). In our slice preparations, astrocytic coupling is probably greatly underestimated, because LY does not spread as far as smaller tracers (e.g., biocytin; Li and Nagy, 2000a), short 5-min labeling periods were used, and dye fixation was unlikely to be fully quantitative (see Materials and Methods). Thus, the size of astrocytic networks and the rate and extent of intercellular transfer in brain in vivo must be substantially higher than generally recognized. The phosphorylation state of Cx43 can enhance or reduce gap junction-mediated

transfer and can change under activating conditions (see the introductory paragraphs), but a physiological stimulus, acoustic activation of the auditory pathway in normal rats, did not cause significant dephosphorylation of Cx43 in the inferior colliculus compared with rest (Fig. 4); thus, extrapolation from one brain region or experimental paradigm to another must be made with caution. Most cells labeled by LY were S100β positive, but the possibility of some dye transfer between astrocytes and oligodendrocytes via heterologous gap junctions (Rash et al., 2001; Nagy et al., 2003) is not ruled out. Notably, the extent of gap junction coupling in slices of inferior colliculus (Table I) is two to three orders of magnitude higher than in cultured cortical astrocytes, which typically range from only approximately five to 40 cells in various studies (e.g., Enkvist and McCarthy, 1992, 1994; Li and Nagy, 2000a; Theis et al., 2003). Cultured astrocytes are useful for various types of studies of gap junctions, but they lack high connectivity and interactions with other cells and are, therefore, not a good model for in vivo metabolic trafficking via the astrocytic syncytium.

The two major astrocytic connexin proteins are abundant in the inferior colliculus, but localization of the immunoreactive connexin proteins and the routinely used astrocytic markers is heterogeneous. The pattern for immunoreactive Cx43 is more similar to that of GFAP, whereas the distributions of Cx30 and S100• are more similar to each other. In general, the staining patterns of Cx43 and GFAP are most predominant in cells near the meninges and aqueduct and on astrocytic processes adjacent to the vasculature, whereas those of Cx30 and S100β are more uniform throughout the inferior colliculus. Both Cx30 and S100β give robust immunolabeling regardless of the tissue or slice preparative procedures, whereas GFAP and Cx43 are quite sensitive to the preparative and fixation methods, as shown in a number of careful studies by Nagy and colleagues (Yamamoto et al., 1990a,b, 1992; Nagy et al., 1999, 2001). Sensitivity of GFAP in the inferior colliculus to the in vitro incubations (Fig. 2) required for post-mortem recovery of brain slice preparations prior to intracellular injections or electrophysiological assays complicates use of this marker for identification of astrocytes and colocalization with fluorescent dyes. Furthermore, low expression of GFAP in the inferior colliculus and its post-mortem changes suggest that fluorescent protein markers linked to the GFAP promoter may not identify the entire astrocyte population in the inferior colliculus in situ, and reactive astrocytic changes may occur in slices with increasing in vitro recovery time. S100β was initially reported to be an astrocytic marker that is not found in neurons (e.g., Ludwin et al., 1976; Cocchia, 1981), but it has been found to be sparsely expressed in some large neurons in the inferior colliculus and other brain regions (Rickmann and Wolff, 1995). In our studies, nearly all of the LY-labeled cells colocalized with S100β and virtually no MAP2-positive cells were dye labeled, indicating indirectly that MAP2 does not colocalize with S100β in these populations (Fig. 5). Compared with GFAP, S100β has the advantage of nuclear and cytoplasmic distribution (Figs. 1, 2), so it is easier to demonstrate colocalization by image overlays after microinjection of LYVS + LYCH. Because of the different astrocyte marker distributions and selective sensitivity to in vitro incubation, no single marker can be used to identify unambiguously all astrocytes in the inferior colliculus or to exclude specific cells from classification as astrocytes.

Potential Impact of Astrocytic Gap Junctional Trafficking on Metabolic Studies

Rapid dye dispersion has important implications for functional brain activation studies in human and animal subjects using [^{11}C-, 13C-, or 14C]glucose in PET, MRS, and autoradiographic assays.

Metabolite Dispersal—Brain regions with highly coupled astrocytes have the capacity to disperse intracellular molecules quickly, widely, and heterogeneously within the time span of brief experimental intervals routinely used for metabolic studies. Diffusion of LY for 5 min labels thousands of astrocytes within a range of 0.3–0.8 mm to a level equal to about half the

concentration of that in the injected cell (Table I, Figs. 5–7), and metabolite distribution of this magnitude is sufficient to contribute to the degradation or loss of registration of focal activation that we observed in 5-min [^{14}C]glucose assays but not during 30–45-min [^{14}C]DG experiments (Cruz et al., 2007). Increased generation of [^{14}C]lactate, transporter-mediated release, and lactate efflux to blood would also contribute to signal loss (Adachi et al., 1995;Cruz et al., 1999,2007). During the longer (0.5–2 hr) labeling intervals employed in PET and MRS studies using [^{11}C- or ^{13}C]glucose, greater metabolite spreading would be anticipated, and the use of various anesthetics to minimize movement artifacts or alter "conscious state" may complicate interpretation of results as a result of differential and dose-dependent impairment of gap junction permeability by some anesthetics (Mantz et al., 1993;Rozental et al., 2001). For example, halothane enhances metabolic trapping in focally activated cells that would otherwise not be detected, as illustrated by improved visualization of [1-^{14}C]glucose-derived tonotopic bands in anesthetized compared with conscious rats (Cruz et al., 2007). To summarize, labeled glucose metabolites that would be retained in astrocytes until they are further metabolized (e.g., glutamate) or more readily released by transporters (e.g., glutamine, lactate, pyruvate, alanine) would be expected to diffuse via intracellular and extracellular routes, thereby influencing results related to glutamate-glutamine cycling, lactate shuttling, and magnitude of focal activation.

Selective Metabolite Retention in Tonotopic Bands—Failure of [^{14}C]DG-6-phosphate to spread from tonotopic bands throughout the entire inferior colliculus (Cruz et al., 2007; Fig. 5A) does not arise from the lack of Cx proteins (Fig. 3), from large changes in overall Cx43 phosphorylation state (Fig. 4), or from low gap junction coupling of astrocytes (Figs. 5–7). Some of the [^{14}C]DG label can be locally retained because of its incorporation into glycogen that is located mainly in astrocytes, but this is a small fraction (~2%) of the [^{14}C]DG metabolite pool (Nelson et al., 1984). Thus, hexose-6-phosphates may be trapped in astrocytes because they are poor substrates for gap junctional transfer, a conclusion that is strongly supported by ongoing studies in our laboratory (Gandhi et al., unpublished). These findings contrast with the report of passage of [1-^{14}C]glucose-6-P through gap junctions (Tabernaro et al., 1996) and the widely held notion that molecules less than ~1 kD readily pass through gap junctions. In fact, our emerging data contribute to the increasing body of evidence for some selectivity of transfer of material through these channels (Nicholson et al., 2000; Harris, 2001; Goldberg et al., 2004; Weber et al., 2004).

The cellular basis of functional metabolic activity in brain has been an unresolved issue for decades because of technical difficulties related to cellular resolution and very high label loss during histological processing (e.g., see Sharp, 1976a,b; Durham et al., 1981); recent estimates suggest that overall glucose utilization rates in astrocytes and neurons are similar under resting conditions (Itoh et al., 2004; Nehlig et al., 2004). Specific neurons are metabolically active even during resting conditions and accumulate high levels of [^{3}H]DG compared with other cells (Duncan et al., 1990), and *increased neuronal trapping* of labeled DG occurs in activated structures in conscious rats during swimming or rotation paradigms (Sharp, 1976a,b). Neurons are not generally gap junction coupled in adult brain (except some GABAergic neurons), and they may metabolize and retain a large fraction of the additional [^{3}H- or ^{14}C]DG accumulated during acoustic activation, thereby contributing to metabolic tonotopic bands. However, if this occurs, the activated neurons must quickly release [^{14}C]metabolites of [1- and 6-^{14}C]glucose, because total ^{14}C-metabolite retention during activation is low compared with that obtained with labeled DG.

Lactate Trafficking and Release From Activated Tissue—Monocarboxylic acid transporter-mediated co-transport of lactate and H^+ from glycolytic cells contributes to control of intracellular pH and helps to maintain high glycolytic rate by removal of acid and lactate. Monocarboxylate transporters are located along the soma, at or near astrocytic endfeet, in

ependymal cells, and in the meninges in adult brain (Gerhart et al., 1997; Leino et al., 1999; Hanu et al., 2000). Thus, labeled lactate and other transportable metabolites can be dispersed by both gap junction- and transporter-mediated trafficking at many sites. Impairment of either of these processes improves visualization of tonotopic bands with [1-^{14}C]glucose (Cruz et al., 2007).

Astrocytic-meningial-perivascular Networks—Dye dispersal from a single astrocyte involves not only distribution within the soma but also within the perivascular gap junction-coupled endfeet that are rapidly and highly labeled at considerable distances from an injected cell (Fig. 7). Accumulation of dye along the perimeter of injected slices (inset, Fig. 5B) raises the possibility of a diffusion barrier that might have arisen because of our removal of the meninges prior to slice preparation. The meninges and the tissue adjacent to both the meninges and the aqueduct are highly enriched in Cx26, Cx30, and Cx43 (Fig. 3; Yamamoto et al., 1990a,b,1992;Nagy et al., 1999,2001), and there is evidence for an extensive meningeoglial network (Mercier and Hatton, 2000); these fluid pathways may help to distribute and remove metabolites from brain. For example, [^{14}C]metabolites released from the soma, fine processes, and endfeet of activated astrocytes via membrane transporters into interstitial fluid have no barrier for diffusion into perivascular fluid in the Virchow-Robin space and into cerebrospinal fluid (Brightman, 2002). The fluid in the Virchow-Robin space is continuous along the entire cerebral vasculature, is propelled by aortic pulsations, and can quickly distribute compounds as large as horseradish peroxidase throughout the brain within minutes (Rennels et al., 1985). Because lactate is a vasoactive compound (Yamanishi et al., 2006), a potential functional role for increased flux of lactate into perivascular fluid during brain activation is regulation of blood flow to working tissue.

CONCLUSIONS

Direct injection of LY into one astrocyte facilitates visualization of a complex, heterogeneous intracellular network connecting a single cell with the vascular and meningial fluid pathways in the inferior colliculus. Activation of thousands of astrocytes during acoustic stimulation of conscious rats in vivo would allow massive syncytial trafficking and extensive intracellular distribution of fuel, metabolites, and signaling compounds according to their concentration gradients. Together, our companion study (Cruz et al., 2007) and the present study implicate gap junctions in spreading of intracellular compounds, thereby contributing to lower signal registration in the tonotopic bands evoked by acoustic stimulation. Conversely, restricted gap junctional transfer of glucose(Glc)-6-phosphate (reflected by [^{14}C]DG-6-P trapping) may be necessary for local regulation of hexokinase activity because of feedback inhibition by Glc-6-P and for control of fluxes of Glc-6-P into the pentose phosphate shunt, glycogen storage, and glycolytic pathways. The role of astrocytic gap junctions in “syncytial sharing” of regulatory, signaling, and high-energy metabolites is an important subject for future studies.

Acknowledgments

Contract grant sponsor: NIH; Contract grant number: NS36728 (to G.D.); Contract grant number: NS47546; Contract grant sponsor: Department of Physiology and Biophysics, and UAMS Graduate School.

REFERENCES

Ackermann RF, Lear JL. Glycolysis-induced discordance between glucose metabolic rates measured with radiolabeled fluorodeoxyglucose and glucose. J Cereb Blood Flow Metab 1989;9:774–785. [PubMed: 2584274]

Adachi K, Cruz NF, Sokoloff L, Dienel GA. Labeling of metabolic pools by [6-^{14}C]glucose during K^+-induced stimulation of glucose utilization in rat brain. J Cereb Blood Flow Metab 1995;15:97–110. [PubMed: 7798343]

Binmöller FJ, Müller CM. Postnatal development of dye-coupling among astrocytes in rat visual cortex. Glia 1992;6:127–137. [PubMed: 1328051]

Brightman MW. The brain's interstitial clefts and their glial walls. J Neurocytol 2002;31:595–603. [PubMed: 14501201]

Bruzzone R, White TW, Paul DL. Connections with connexins: the molecular basis of direct intercellular signaling. Eur J Biochem 1996;238:1–27. [PubMed: 8665925]

Cocchia D. Immunocytochemical localization of S-100 protein in the brain of adult rat. An ultrastructural study. Cell Tissue Res 1981;214:529–540. [PubMed: 7214465]

Collins RC, McCandless DW, Wagman IL. Cerebral glucose utilization: comparison of [^{14}C] deoxyglucose and [6-^{14}C]glucose quantitative autoradiography. J Neurochem 1987;49:1564–1570. [PubMed: 3668540]

Cruz NF, Dienel GA. High glycogen levels in brains of rats with minimal environmental stimuli: implications for metabolic contributions of working astrocytes. J Cereb Blood Flow Metab 2002;22:1476–1489. [PubMed: 12468892]

Cruz NF, Adachi K, Dienel GA. Metabolite trafficking during K^+-induced spreading cortical depression: rapid efflux of lactate from cerebral cortex. J Cereb Blood Flow Metab 1999;19:380–392. [PubMed: 10197508]

Cruz NF, Ball KK, Dienel GA. Functional imaging of focal brain activation in conscious rats: impact of [^{14}C]glucose metabolite spreading and release. J Neurosci Res 2007;85:3254–3266. [PubMed: 17265468]

D'Ambrosio R, Wenzel J, Schwartzkroin PA, McKhann GM 2nd, Janigro D. Functional specialization and topographic segregation of hippocampal astrocytes. J Neurosci 1998;18:4425–4438. [PubMed: 9614220]

Dienel GA, Cruz NF. Nutrition during brain activation: does cell-to-cell lactate shuttling contribute significantly to sweet and sour food for thought? Neurochem Int 2004;45:321–351. [PubMed: 15145548]

Dienel GA, Cruz NF. Astrocyte activation in working brain: energy supplied by minor substrates. Neurochem Int 2006;48:586–595. [PubMed: 16513214]

Dienel GA, Wang RY, Cruz NF. Generalized sensory stimulation of conscious rats increases labeling of oxidative pathways of glucose metabolism when the brain glucose-oxygen uptake ratio rises. J Cereb Blood Flow Metab 2002;22:1490–1502. [PubMed: 12468893]

Duncan GE, Kaldas RG, Mitra KE, Breese GR, Stumpf WE. High activity neurons in the reticular formation of the medulla oblongata: a high-resolutionautoradiographic2-deoxyglucosestudy. Neuroscience 1990;35:593–600. [PubMed: 2381517]

Durham D, Woolsey TA, Kruger L. Cellular localization of 2-[^{3}H]deoxy-D-glucose from paraffin-embedded brains. J Neurosci 1981;1:519–526. [PubMed: 7346567]

Enkvist MO, McCarthy KD. Activation of protein kinase C blocks astroglial gap junction communication and inhibits the spread of calcium waves. J Neurochem 1992;59:519–526. [PubMed: 1629725]

Enkvist MO, McCarthy KD. Astroglial gap junction communication is increased by treatment with either glutamate or high K^+ concentration. J Neurochem 1994;62:489–495. [PubMed: 7905024]

Gerhart DZ, Enerson BE, Zhdankina OY, Leino RL, Drewes LR. Expression of monocarboxylate transporter MCT1 by brain endothelium and glia in adult and suckling rats. Am J Physiol 1997;273:E207–E213. [PubMed: 9252498]

Giaume C, McCarthy KD. Control of gap-junctional communication in astrocytic networks. Trends Neurosci 1996;19:319–325. [PubMed: 8843600]

Giaume C, Tabernero A, Medina JM. Metabolic trafficking through astrocytic gap junctions. Glia 1997;21:114–123. [PubMed: 9298854]

Goldberg GS, Valiunas V, Brink PR. Selective permeability of gap junction channels. Biochim Biophys Acta 2004;1662:96–101. [PubMed: 15033581]

Gross PM, Sposito NM, Pettersen SE, Fenstermacher JD. Differences in function and structure of the capillary endothelium in gray matter, white matter and a circumventricular organ of rat brain. Blood Vessels 1986;23:261–270. [PubMed: 3790742]

Gross PM, Sposito NM, Pettersen SE, Panton DG, Fenstermacher JD. Topography of capillary density, glucose metabolism, and microvascular function within the rat inferior colliculus. J Cereb Blood Flow Metab 1987;7:154–160. [PubMed: 3558498]

Hafidi A, Galifianakis D. Macroglia distribution in the developing and adult inferior colliculus. Brain Res Dev Brain Res 2003;143:167–177.

Hanu R, McKenna M, O'Neill A, Resneck WG, Bloch RJ. Monocarboxylic acid transporters, MCT1 and MCT2, in cortical astrocytes in vitro and in vivo. Am J Physiol Cell Physiol 2000;278:C921–C930. [PubMed: 10794666]

Harris AL. Emerging issues of connexin channels: biophysics fills the gap. Q Rev Biophys 2001;34:325–472. [PubMed: 11838236]

Hossain MZ, Murphy LJ, Hertzberg EL, Nagy JI. Phosphorylated forms of connexin43 predominate in rat brain: demonstration by rapid inactivation of brain metabolism. J Neurochem 1994;62:2394–2403. [PubMed: 8189244]

Inagaki M, Kaga M, Isumi H, Hirano S, Takashima S, Nanba E. Hypoxia-induced ABR change and heat shock expression in the pontine auditory pathway of young rabbits. Brain Res 1997;757:111–118. [PubMed: 9200505]

Itoh Y, Abe T, Takaoka R, Tanahashi N. Fluorometric determination of glucose utilization in neurons in vitro and in vivo. J Cereb Blood Flow Metab 2004;24:993–1003. [PubMed: 15356420]

Konietzko U, Müller CM. Astrocytic dye coupling in rat hippocampus: topography, developmental onset, and modulation by protein kinase C. Hippocampus 1994;4:297–306. [PubMed: 7842053]

Lampe PD, Lau AF. The effects of connexin phosphorylation on gap junctional communication. Int J Biochem Cell Biol 2000;36:1171–1186. [PubMed: 15109565]

Lampe PD, TenBroek EM, Burt JM, Kurata WE, Johnson RG, Lau AF. Phosphorylation of connexin43 on serine368 by protein kinase C regulates gap junctional communication. J Cell Biol 2000;149:1503–1512. [PubMed: 10871288]

Lear JL, Ackermann RF. Comparison of cerebral glucose metabolic rates measured with fluorodeoxyglucose and glucose labeled in the 1, 2, 3–4, and 6 positions using double label quantitative digital autoradiography. J Cereb Blood Flow Metab 1988;8:575–585. [PubMed: 3392117]

Lear J, Ackermann RF. Why the deoxyglucose method has proven so useful in cerebral activation studies: the unappreciated prevalence of stimulation-induced glycolysis. J Cereb Blood Flow Metab 1989;9:911–913. [PubMed: 2584281]

Lear, J.; Ackermann, R. Autoradiographic comparison of FDG-based and GLU-based measurements of cerebral glucose transport and metabolism: normal and activated conditions. In: Lassen, N.; Ingvar, D.; Raichle, M.; Friberg, L., editors. Brain work and mental activity, Alfred Benzon Symposium 31; Copenhagen: Munskgaard; 1991. p. 142-152.

Leino RL, Gerhart DZ, Drewes LR. Monocarboxylate transporter (MCT1) abundance in brains of suckling and adult rats: a quantitative electron microscopic immunogold study. Brain Res Dev Brain Res 1999;113:47–54.

Li WE, Nagy JI. Connexin43 phosphorylation state and intercellular communication in cultured astrocytes following hypoxia and protein phosphatase inhibition. Eur J Neurosci 2000a;12:2644–2650. [PubMed: 10947839]

Li WE, Nagy JI. Activation of fibres in rat sciatic nerve alters phosphorylation state of connexin-43 at astrocytic gap junctions in spinal cord: evidence for junction regulation by neuronal–glial interactions. Neurosci 2000b;97:113–123.

Li WE, Ochalski PA, Hertzberg EL, Nagy JI. Immunorecognition, ultrastructure and phosphorylation status of astrocytic gap junctions and connexin43 in rat brain after cerebral focal ischaemia. Eur J Neurosci 1998;10:2444–2463. [PubMed: 9749772]

Loewenstein WR. Junctional intercellular communication: the cell-to-cell membrane channel. Physiol Rev 1981;61:829–913. [PubMed: 6270711]

Ludwin SK, Kosek JC, Eng LF. The topographical distribution of S-100 and GFA proteins in the adult rat brain: an immunohistochemical study using horseradish peroxidase-labelled antibodies. J Comp Neurol 1976;165:197–207. [PubMed: 1107363]

Mantz J, Cordier J, Giaume C. Effects of general anesthetics on intercellular communications mediated by gap junctions between astrocytes in primary culture. Anesthesiology 1993;78:892–901. [PubMed: 7683851]

Marrero H, Orkand RK. Nerve impulses increase glial intercellular permeability. Glia 1996;16:285–289. [PubMed: 8833199]

Mercier F, Hatton GI. Immunocytochemical basis for a meningeoglial network. J Comp Neurol 2000;420:445–465. [PubMed: 10805920]

Moyer JR Jr, Brown TH. Methods for whole-cell recording from visually preselected neurons of perirhinal cortex in brain slices from young and aging rats. J Neurosci Methods 1998;86:35–54. [PubMed: 9894784]

Nagy JI, Li WE. A brain slice model for in vitro analyses of astrocytic gap junction and connexin43 regulation: actions of ischemia, glutamate and elevated potassium. Eur J Neurosci 2000;12:4567–4572. [PubMed: 11122370]

Nagy JI, Rash JE. Connexins and gap junctions of astrocytes and oligodendrocytes in the CNS. Brain Res Brain Res Rev 2000;32:29–44. [PubMed: 10751655]

Nagy JI, Rash JE. Astrocyte and oligodendrocyte connexins of the glial syncytium in relation to astrocyte anatomical domains and spatial buffering. Cell Commun Adhes 2003;10:401–406. [PubMed: 14681048]

Nagy JI, Patel D, Ochalski PAY, Stelmack GL. Connexin30 in rodent, cat and human brain: selective expression in gray matter astrocytes, co-localization with connexin43 at GAP junctions and late developmental appearance. Neuroscience 1999;88:447–468. [PubMed: 10197766]

Nagy JI, Li X, Rempel J, Stelmack G, Patel D, Staines WA, Yasumura T, Rash JE. Connexin26 in adult rodent central nervous system: demonstration at astrocytic gap junctions and co-localization with connexin30 and connexin43. J Comp Neurol 2001;441:302–323. [PubMed: 11745652]

Nagy JI, Ionescu AV, Lynn BD, Rash JE. Coupling of astrocyte connexins Cx26, Cx30, Cx43 to oligodendrocyte Cx29, Cx32, Cx47: Implications from normal and connexin32 knockout mice. Glia 2003;44:205–218. [PubMed: 14603462]

Nehlig A, Wittendorp-Rechenmann E, Lam CD. Selective uptake of [^{14}C]2-deoxyglucose by neurons and astrocytes: high-resolution microautoradiographic imaging by cellular ^{14}C-trajectography combined with immunohistochemistry. J Cereb Blood Flow Metab 2004;24:1004–1014. [PubMed: 15356421]

Nelson T, Kaufman EE, Sokoloff L. 2-Deoxyglucose incorporation into rat brain glycogen during measurement of local cerebral glucose utilization by the 2-deoxyglucose method. J Neurochem 1984;43:949–956. [PubMed: 6470715]

Nicholson BJ, Weber PA, Cao F, Chang H, Lampe P, Goldberg G. The molecular basis of selective permeability of connexins is complex and includes both size and charge. Braz J Med Biol Res 2000;33:369–378. [PubMed: 10775301]

Rash JE, Yasumura T, Dudek FE, Nagy JI. Cell-specific expression of connexins and evidence of restricted gap junctional coupling between glial cells and between neurons. J Neurosci 2001;21:1983–2000. [PubMed: 11245683]

Rennels ML, Gregory TF, Blaumanis OR, Fujimoto K, Grady PA. Evidence for a “paravascular” fluid circulation in the mammalian central nervous system, provided by the rapid distribution of tracer protein throughout the brain from the subarachnoid space. Brain Res 1985;326:47–63. [PubMed: 3971148]

Rickmann M, Wolff JR. S100 protein expression in subpopulations of neurons of rat brain. Neuroscience 1995;67:977–991. [PubMed: 7675218]

Rouach N, Koulakoff A, Giaume C. Neurons set the tone of gap junctional communication in astrocytic networks. Neurochem Int 2004;45:265–272. [PubMed: 15145542]

Rozental R, Srinivas M, Spray DC. how to close a gap junction. Efficacies and potencies of uncoupling agents. Methods Mol Biol 2001;154:447–476. [PubMed: 11218664]

Sharp FR. Relative cerebral glucose uptake of neuronal perikarya and neuropil determined with 2-deoxyglucose in resting and swimming rat. Brain Res 1976a;110:127–139. [PubMed: 1276944]

Sharp FR. Rotation induced increases of glucose uptake in rat vestibular nuclei and vestibulocerebellum. Brain Res 1976b;110:141–151. [PubMed: 1276945]

Simard M, Arcuino G, Takano T, Liu QS, Nedergaard M. Signaling at the gliovascular interface. J Neurosci 2003;23:9254–9262. [PubMed: 14534260]

Simpson I, Rose B, Loewenstein WR. Size limit of molecules permeating the junctional membrane channels. Science 1977;195:294–296. [PubMed: 831276]

Sokoloff L, Reivich M, Kennedy C, Des Rosiers MH, Patlak CS, Pettigrew KD, Sakurada O, Shinohara M. The [^{14}C]deoxyglucose method for the measurement of local glucose utilization: theory, procedure, and normal values in the conscious and anesthetized albino rat. J Neurochem 1977;28:897–916. [PubMed: 864466]

Sternberger, LA. Immunocytochemistry. 2nd ed.. John Wiley & Sons; New York: 1979.

Stewart WW. Lucifer dyes—highly fluorescent dyes for biological tracing. Nature 1981;292:17–21. [PubMed: 6168915]

Tabernero A, Giaume C, Medina JM. Endothelin-1 regulates glucose utilization in cultured astrocytes by controlling intercellular communication through gap junctions. Glia 1996;16:187–195. [PubMed: 8833189]

Theis M, Jauch R, Zhuo L, Speidel D, Wallraff A, Doring B, Frisch C, Sohl G, Teubner B, Euwens C, Huston J, Steinhauser C, Messing A, Heinemann U, Willecke K. Accelerated hippocampal spreading depression and enhanced locomotory activity in mice with astrocyte-directed inactivation of connexin43. J Neurosci 2003;23:766–776. [PubMed: 12574405]

Weber PA, Chang HC, Spaeth KE, Nitsche JM, Nicholson BJ. The permeability of gap junction channels to probes of different size is dependent on connexin composition and permeant-pore affinities. Biophys J 2004;87:958–973. [PubMed: 15298902]

Yamamoto T, Ochalski A, Hertzberg EL, Nagy JI. On the organization of astrocytic gap junctions in the rat brain as suggested by LM and EM immunohistochemistry of connexin43 expression. J Comp Neurol 1990a;302:853–883. [PubMed: 1964467]

Yamamoto T, Ochalski A, Hertzberg EL, Nagy JI. LM and EM immunolocalization of the gap junctional protein connexin 43 in rat brain. Brain Res 1990b;508:313–319. [PubMed: 2155040]

Yamamoto T, Vukelic J, Hertzberg EL, Nagy JI. Differential anatomical and cellular patterns of connexin43 expression during postnatal development of rat brain. Brain Res Dev Brain Res 1992;66:165–180.

Yamanishi S, Katsumura K, Kobayashi T, Puro DG. Extracellular lactate as a dynamic vasoactive signal in the rat retinal microvasculature. Am J Physiol Heart Circ Physiol 2006;290:H925–H934. [PubMed: 16299264]

Zahs KR, Newman EA. Asymmetric gap junctional coupling between glial cells in the rat retina. Glia 1997;20:10–22. [PubMed: 9145301]

Zahs KR, Wu T. Confocal microscopic study of glial–vascular relationships in the retinas of pigmented rats. J Comp Neurol 2001;429:253–269. [PubMed: 11116218]

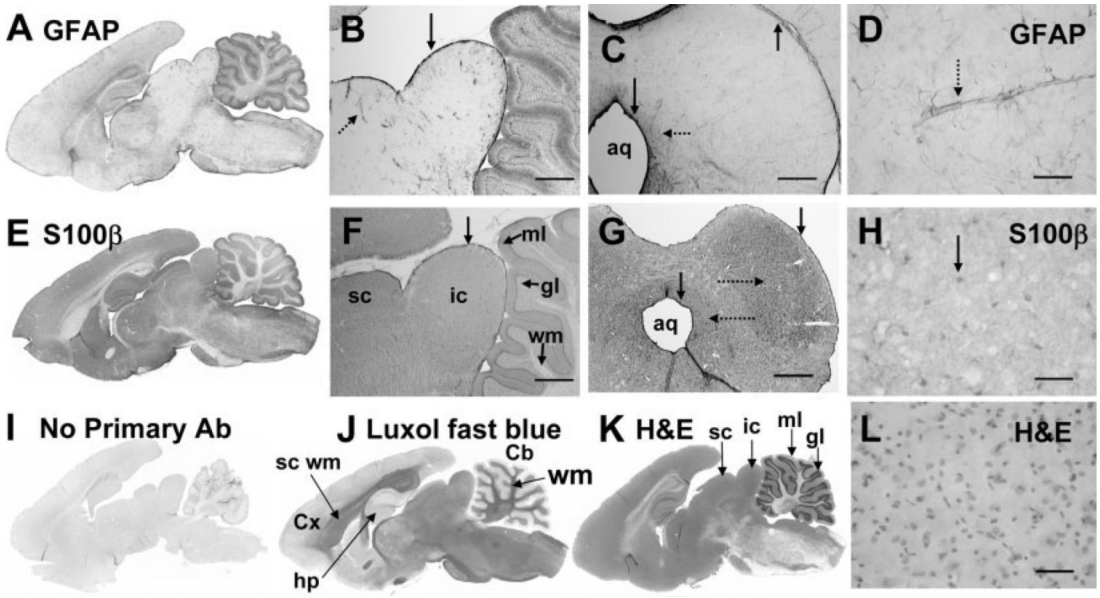

Fig. 1.

Immunoreactive glial fibrillary acidic protein (GFAP) and S100β in adult rat brain. Sagittal sections of adult rat brain showing the heterogeneous distributions of immunoreactive GFAP (**A**) and S100β (**E**) compared with 1) low staining by the secondary antibody when the primary antibody was omitted (**I**), 2) staining of myelin by luxol fast blue (**J**), and 3) cellular staining by hematoxylin and eosin (H&E; **K**). Higher-power sagittal (**B,F**) and coronal (**C,D** and **G,H**) sections compare GFAP (B–D) and S100β (F–H) staining with H&E cell stain (**L**). Note the intense immunostaining of both GFAP and S100β in the meninges along the surface of the inferior colliculus (vertical arrows, B,C,F,G) and in the cells adjacent to the aqueduct (aq; vertical arrows, C,G). The parenchyma surrounding the aqueduct (leftward-facing horizontal dotted arrows, C,G) is also more heavily stained by both antibodies, and immunoreactive S100β is somewhat more dense in the central zone of the inferior colliculus (rightward-facing dotted arrow, G). GFAP staining is most intense around blood vessels (dotted arrows, B,D) and is much lower in neuropil (A–D). S100β staining is more uniform throughout the neuropil but is more intense in nuclei (arrow, H) compared with cytoplasm; it is also evident in perivascular structures (not shown, see Fig. 7). All immunostaining used the PAP procedure with DAB (see Materials and Methods). Cx, cerebral cortex; sc wm, subcortical white matter; hp, hippocampus; Cb, cerebellum; wm, white matter; sc, superior colliculus; ic, inferior colliculus; ml, molecular layer of cerebellum; gl, granular layer of cerebellum; aq, aqueduct. Scale bars = 800 μm in B,C,F,G; 50 μm in D,H,L.

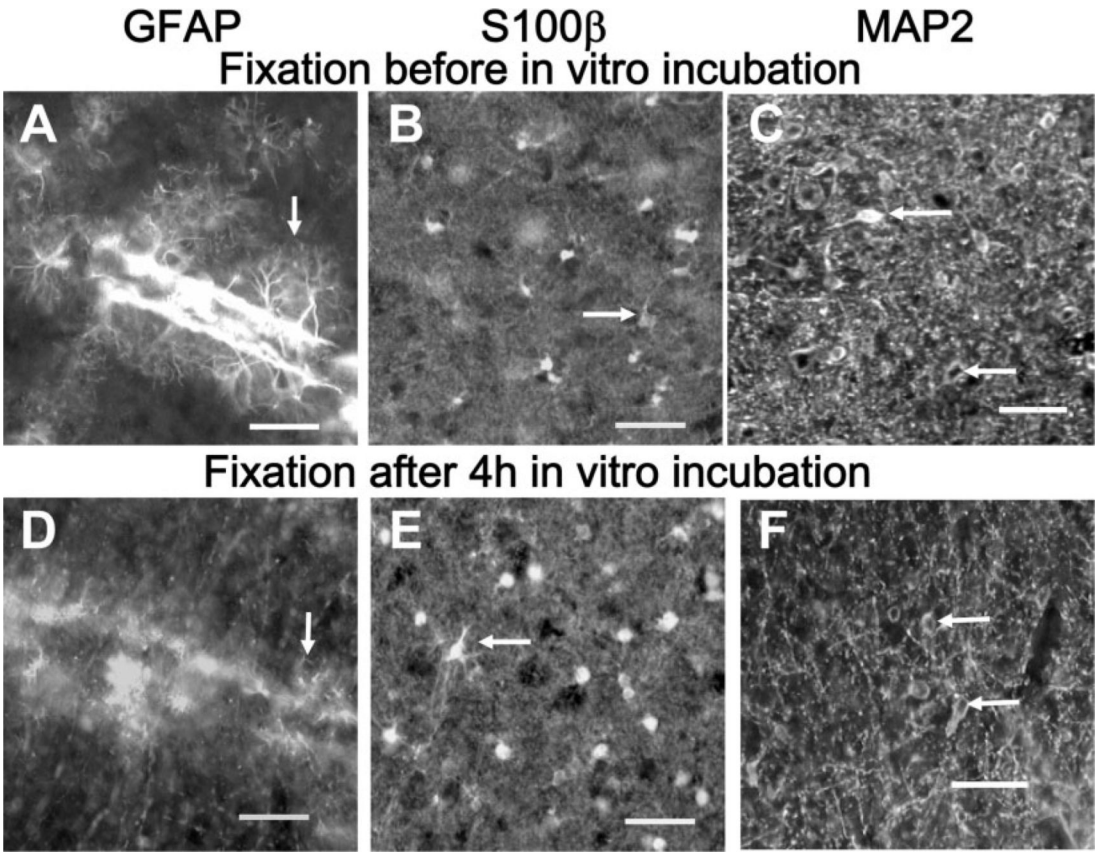

Fig. 2.

Loss of immunoreactive GFAP after in vitro incubation of slices of inferior colliculus. Tissue slices (250 μm thick) were immersion fixed in 4% paraformaldehyde either immediately after slicing (**A–C**) or 4 hr after slicing and in vitro incubation (**D–F**), then assayed for immunoreactive GFAP (A,D), S100β (B,E), or MAP2 (C,F; all images were obtained by use of fluorescent secondary antibodies; see Materials and Methods). Note loss of fine immunoreactive GFAP-positive processes when fixation is delayed (compare A and D, arrows), whereas staining of nuclei and processes by anti-S100β (arrows, B,E) and neuronal staining by anti-MAP2 (arrows, C,F) were not substantially altered by the slice-recovery incubation procedure. Scale bars = 50 μm.

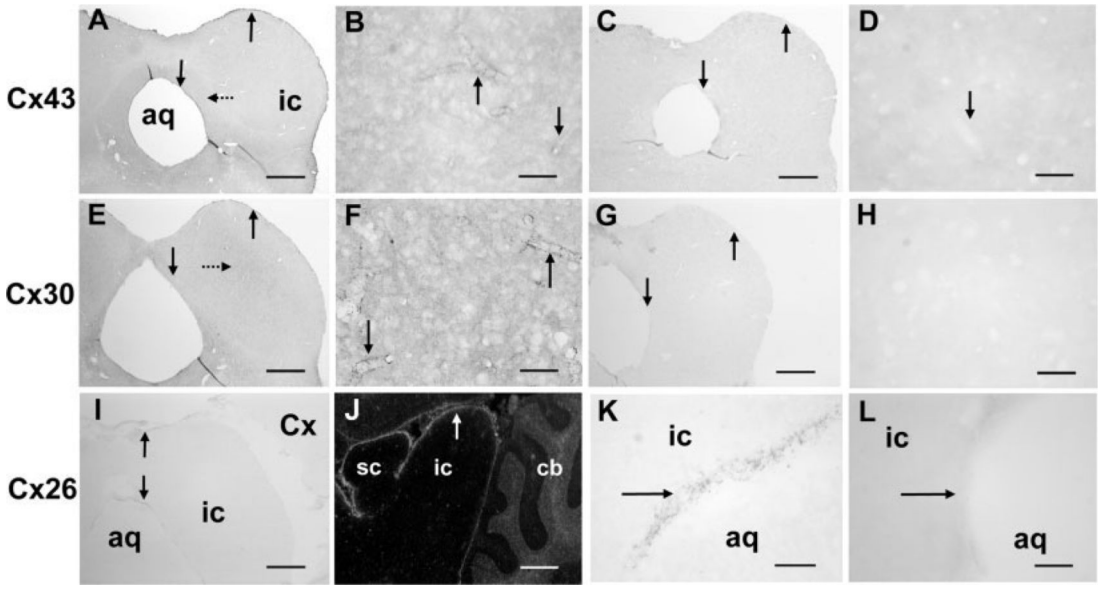

Fig. 3.

Immunoreactive Cx43, Cx30, and Cx26 in the inferior colliculus of the adult rat. Coronal sections at the level of midinferior colliculus (except the sagittal section, J) illustrate the distributions of immunoreactive Cx43 (**A,B**), Cx30 (**E,F**), and Cx26 (**I–K**) compared with the respective controls in which the primary antibody was omitted (**C,D,G,H,L**). Vertical arrows indicate highest staining in the meninges, cells surrounding the aqueduct and around blood vessels (A,B,E,F,I,J), which is low in the control sections (C,D,G,H,L); note that immunoreactive Cx30 is somewhat higher in the central zone of inferior colliculus (dotted arrow, E). The PAP method was used for immunostaining, except in J, where a fluorescent secondary antibody was used to visualize the very faint staining of Cx26 in the meninges and in cells around the aqueduct (arrows, I–K). Because Nagy et al. (2001) reported 1) very high levels of Cx26 protein in Western blots of extracts from superior and inferior colliculus after separation by gel electrophoresis, 2) immunofluorescence labeling of superficial layers of superior colliculus and the cerebellar granular layer, and 3) sparse distribution in the molecular layer that contrasted the low immunostaining in superior and inferior colliculus (but note that cortical and cerebellar staining observed in the present study, Fig. 3J was similar to the Nagy et al. findings), Cx26 was also assayed with various primary antibody dilutions (1:12.5, 1:20, 1:50, 1:100, 1:200) and with different preparative methods (perfusion-fixed tissue, in slices fixed immediately by immersion, air-dried fresh-frozen slices that were not fixed or were fixed in methanol or acetone), but no improvement in staining of the inferior colliculus could be obtained (data not shown). aq, Aqueduct; ic, inferior colliculus; sc, superior colliculus; Cx, cerebral cortex; cb, cerebellum. Scale bars = 800 μm in A,C,E,G,I,J; 50 μm in B,D,F,H,K,L.

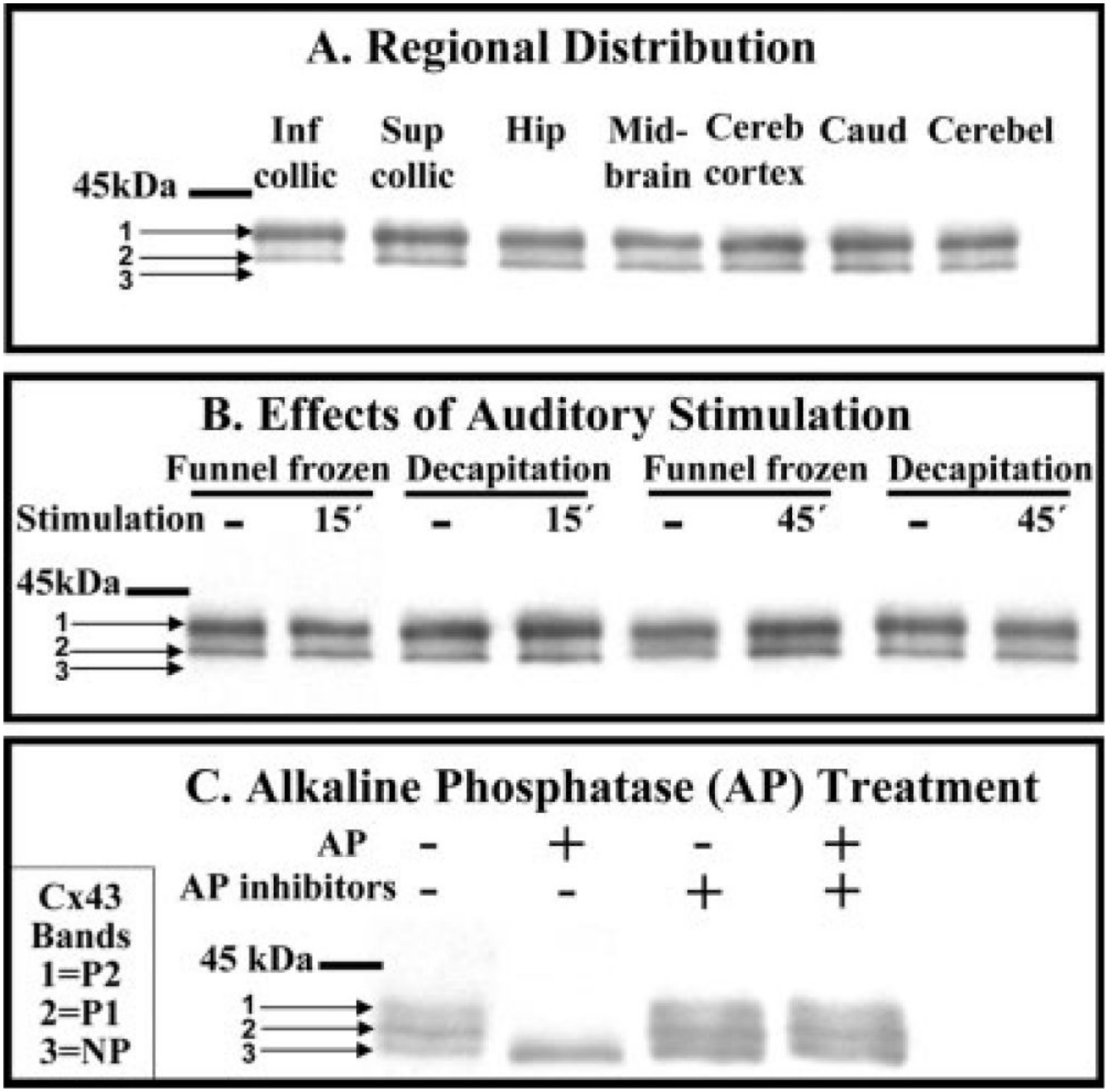

Fig. 4.

Highly phosphorylated Cx43 is the predominant isoform in the inferior colliculus during rest and after acoustic stimulation. **A**: Cx43 isoforms in seven brain regions. **B**: Phosphorylation state of Cx43 before (dashes indicated "resting" rats) and after 15 or 45 min of acoustic stimulation (40 Hz to 8 kHz broadband stimulus) of conscious rats; tissue was sampled from inferior colliculus by dissection from brain tissue that was frozen in situ (funnel frozen) or obtained after decapitation (see Materials and Methods). **C**: Brain homogenates were incubated in vitro in the presence or absence of alkaline phosphatase (AP) or AP inhibitors (fluoride plus vanadate) prior to separation on SDS-PAGE gels, Western blotting, and immunostaining (see Materials and Methods). Pretreatment of the Zymed antibody with the Zymed Cx43 peptide completely blocked Cx43 immunostaining (not shown). NP denotes nonphosphorylated Cx43,

whereas P1 and P2 denote phosphorylated isoforms; the horizontal bar indicates the position of 45-kDa molecular weight standard. Inf collic, inferior colliculus; Sup collic, superior colliculus; Hip, hippocampus; Cereb, cerebral; Caud, caudate; Cerebel, cerebellum; AP, alkaline phosphatase, Cx43, connexin 43.

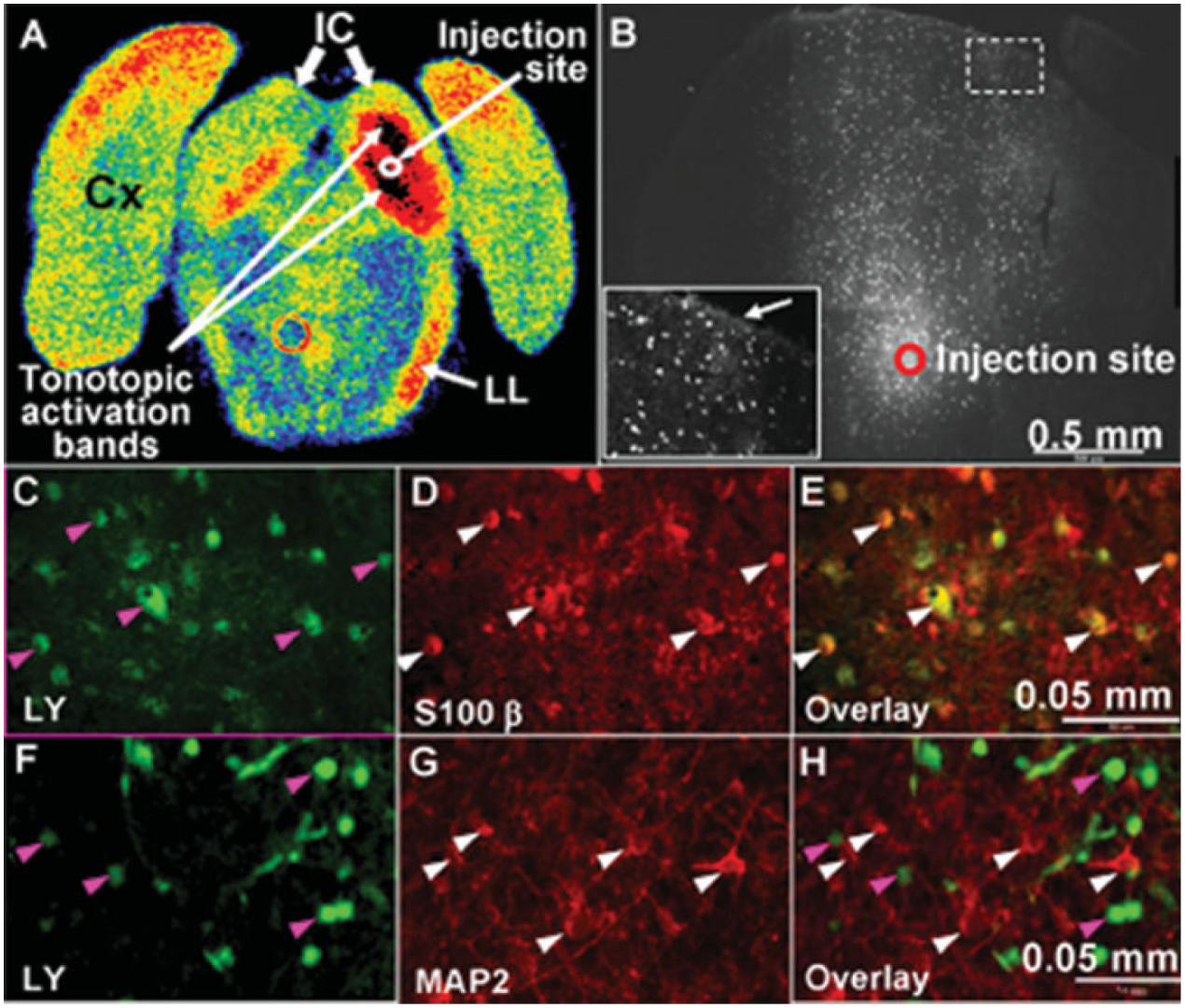

Fig. 5.

Rapid, extensive transfer of Lucifer yellow among astrocytes in slices of inferior colliculus. **A**: Autoradiograph of coronal section of rat brain at the level of the inferior colliculus after in vivo metabolic imaging with the [^{14}C]DG method during unilateral monotonic auditory stimulation (8 kHz at 103 dB, one ear blocked) to stimulate glucose utilization in the auditory pathway in the right hemisphere (see Cruz et al., 2007). Color coding represents glucose utilization rate (high to low: black, red, orange, yellow, green, blue). Note the high rates of glucose utilization represented by the two black tonotopic activation bands in the right inferior colliculus (IC); the red band in the lower medial region of the left inferior colliculus probably arose from crossover of auditory fibers. Activation is also evident in the right lateral lemniscus (LL). Cx denotes cerebral cortex. **B**: A single astrocyte in a brain slice was microinjected with Lucifer yellow (LY; 4% LYVS + 4% LYCH), approximately in the center of the inferior colliculus as indicated in A, and the dye was allowed to diffuse from the pipette for 5 min. LY-labeled cells coupled to an injected astrocyte via gap junctions are shown in B, C, and F; the **inset** in B is a higher magnification view of a region distant from the injection site (dashed box) near the meninges. Note the bright labeling at the tissue boundary (arrow in inset, B), suggesting a diffusion barrier. Immunohistochemical staining identified LY-labeled cells (green) in **C** and **F** as astrocytes by colocalization with S100β (**D,E**) but not MAP2 (**G,H**).

Arrowheads identify specific cells in these panels; similar results were obtained with immunostaining of three replicate preparations. Scale bars = 0.05 mm.

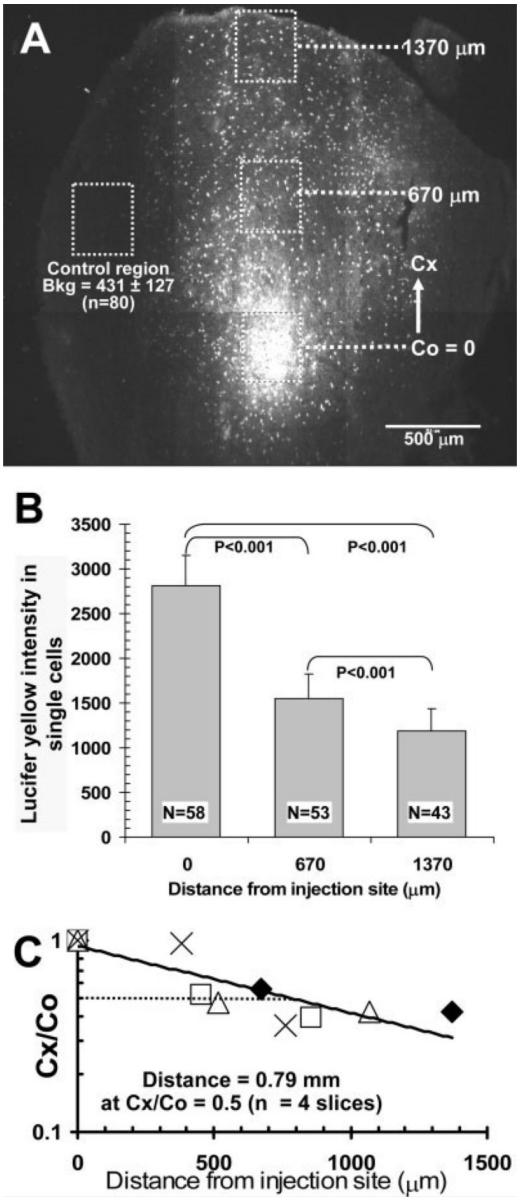

Fig. 6.

Relative fluorescence intensity of Lucifer yellow in gap junction-coupled astrocytes as function of distance from injection site. **A**: Representative montage showing the site where a single astrocyte in a slice of inferior colliculus was microinjected with 4% Lucifer yellow (LY) VS + 4% LYCH and allowed to diffuse for 5 min. Boxes (300 × 300 μm) were drawn around the dye-labeled cells and at various distances from the injection site. Cx denotes the distance from the center of the box surrounding the injection site (Co) to the center of a box located at various distances ranging from about 0.4 to1.4 mm from the injection site in different brain slices; in this representative figure, Cx = 0.67 and 1.37 mm. **B**: Single LY-labeled astrocytes within each box in A were outlined in MetaVue software to determine their fluorescence intensities. The maximal intensity to saturate the camera is about 4,000 fluorescence units. By visual inspection, the peak intensity in the cells assayed was below the saturation value, but the possibility of differential fluorescence quenching in the labeled cells as a function of distance was not evaluated. Values are means for the number of cells indicated and correspond to cells located

in the respective boxes shown in A; vertical lines = 1 SD. The fluorescence intensities among all groups were statistically significantly different (ANOVA, Bonferroni test). Note that the mean intensity of cells located about 1.4 mm from the injection site was about three times higher than background (Bkg.) fluorescence determined in a control region (dotted box, A) that had few, if any, cells labeled by dye transfer; the parenchyma and blood vessels in this region had low levels of autofluorescence after paraformaldehyde fixation. **C**: Semi-log plot of the Cx/Co ratio for the mean LY fluorescence intensities in cells located at various distances from the injection site in four slices. In each slice (indicated by a different symbol), cells were counted in each of three boxes as shown in A,B, and Cx/Co ratios were calculated for each slice using mean values for cells in each box. The distance at which the fluorescence intensity fell by 50% (Cx/Co = 0.5) was calculated to be 0.79 mm, from the equation of the regression line, i.e., $y = 0.937e^{-0.0008x}$ ($R^2 = 0.749$), based on the data from four slices. If the cells with the high levels of LY did have some quenching, the Co values would be underestimated, causing overestimation of the Cx/Co ratios and of the calculated distance at which Cx/Co = 0.5; this distance estimate is, therefore, a maximal value. For example, if all Co values were underestimated by a factor of two, the regression line in C would be $y = 0.809e^{-0.0014x}$ ($R^2 = 0.791$), and calculated distance for Cx/Co = 0.5 is 0.34 mm.

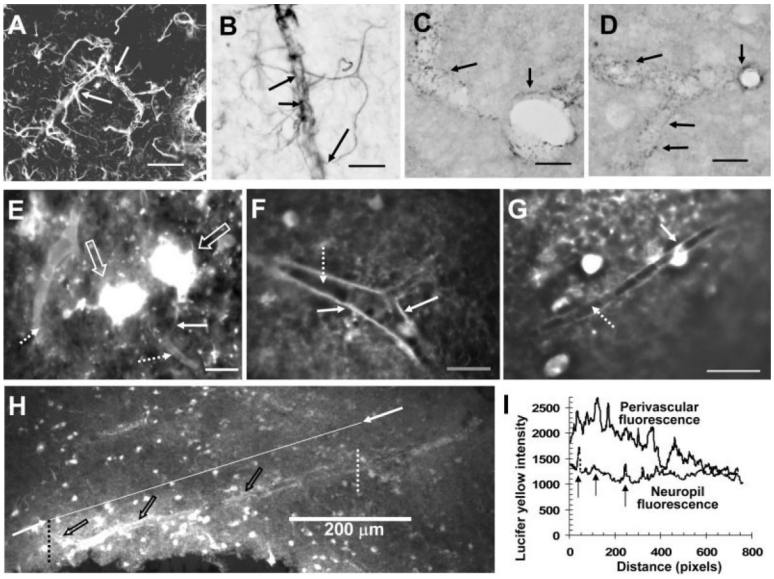

Fig. 7.

Perivascular spread of Lucifer yellow after injection of a single astrocyte. Astrocytes in close contact with the microvasculature were readily identified via their contents of immunoreactive glial fibrillary acidic protein (GFAP), using either a fluorescent secondary antibody (**A**, arrows indicate two astrocytes with processes along the vessel and in the parenchyma) or the PAP method with DAB staining (**B**, arrows indicate endfeet attached to astrocytic processes near a vessel). Punctate staining of gap junction proteins (arrows) around blood vessels shown in cross-section or longitudinal section was readily detected with the PAP method and DAB staining of immunoreactive Cx43 (**C**) and Cx30 (**D**; see Materials and Methods). **E–H** illustrate perivascular localization of Lucifer yellow after microinjection of a single astrocyte. E: One of the highly fluorescent astrocytes (large arrows) has a fine process (solid arrow) that extends toward a blood vessel that is one of two vessels surrounded by Lucifer yellow (dotted arrows). Perivascular labeling of vessels in cross-section show outlining at a bifurcation (F, solid arrow), with heterogeneous fluorescence intensity along the wall of the vessel that appears to be highest in the vicinity of an astrocytic process (G, solid arrow); note the lack of labeling in the lumen of the vessels (F,G, dotted arrows). The relative intensity of perivascular labeling by Lucifer yellow compared with adjacent tissue (H) after injection of a single astrocyte is illustrated by the intensity line scans determined with MetaVue software (**I**) that were drawn from left to right along the upper boundary of the vessel wall (open arrows; denoted as perivascular fluorescence in I) between the dotted vertical lines in H or through the parenchyma along the line connecting the two arrows shown in H and denoted as neuropil fluorescence. Note that the fluorescence intensity along the vessel wall decreased with distance left to right; it was heterogeneous and, over a substantial distance, was about twice that of parenchyma (I); higher perivascular vs. parenchymal labeling is also evident in E–G. Note the intermittent “spike” increases in fluorescence intensity (vertical arrows) as the tissue scan line passes from left to right through highly labeled astrocytes in the neuropil (compare H and I). In line scans made along seven additional blood vessels located within the range of about 0.7–1.2 mm from the injection site, the perivascular Lucifer yellow fluorescence varied in intensity as illustrated in H,I; the perivascular regions with high fluorescence intensity exceeded that of the adjacent neuropil by a factor of 1.7 ± 0.3 (mean ± SD, n = 7). Scale bars = 50 μm in A; 20 μm in B–G; 200 μm in H.

TABLE I

Properties of Astrocytic Syncytia Labeled by Microinjection of Lucifer Yellow (LY) Into One Astrocyte in a Slice of Inferior Colliculus and a 5-Min Dye Diffusion Interval[†]

Number of cells labeled by various concentrations of Lucifer yellow	
8% LYVS	6,101 ± 4,134 (n = 7)
Range	2,068–11,939
4% LYVS + 4% LYCH	2,204 ± 1,482 (n = 11)[*]
Range	544–4,801
4% LYVS + 4% LYCH after octanol pretreatment	13 ± 6 (n = 6)[***]
2% LYVS + 2% LYCH	321 ± 212 (n = 4)[**]
Range	143–615
Maximal distance of 4% LYVS + 4% LYCH spread from injected cell	0.62 ± 0.30 mm (n = 11)
Range	0.21–1.29 mm
Volume containing the 4% LYVS + 4% LYCH dye-labeled syncytium in a slice	0.008 ± 0.006 mm^3 (n = 11)
Volume of ipsilateral inferior colliculus in a slice	1.1 ± 0.1 mm^3 (n = 11)
Colocalization of Lucifer yellow with cell type markers	Cell counts per group
Lucifer yellow-labeled/S100β-labeled/Colocalized	278/291/271
Lucifer yellow-labeled/MAP2-labeled/Colocalized	330/86/1

[†]A single astrocyte located approximately in the center of the inferior colliculus (see Fig. 5A, B) in 250-μm-thick slices from brains of adult rats was microinjected with a pipette containing various concentrations of Lucifer yellow (LY) VS and LYCH with or without octanol pretreatment (0.6 mM for 10 min) to block gap junctions. Five minutes later, the pipette was quickly withdrawn, the slice immediately fixed in 4% paraformaldehyde; serial 20-μm-thick coronal sections of each slice were cut, and the number of labeled cells was counted in each section and summed for each slice. Values are means ± SD (n = number of slices). For slices injected with 4% LYVS + 4% LYCH, the maximal distance from the injected cell to the furthest visibly labeled cell was measured and, for each section, the tissue area containing the labeled cells and the area of the inferior colliculus in that hemisphere were determined in MetaVue software. For each slice, the volume containing the Lucifer yellow-labeled astrocytic syncytium and volume of ipsilateral inferior colliculus were calculated for each slice as the sum of the products of respective areas times the 20-μm section thickness. Fixed slices were stained for S100β (predominant astrocytic marker) or MAP2 (neuronal marker) by immunohistochemistry (Fig. 5C–H), and their colocalization with Lucifer yellow was assessed by cell counts in eight slices for S100β or seven slices for MAP2; for each marker, the slices were from three or four rats, respectively. In slices immunostained for S100β, seven of the 278 Lucifer yellow-labeled cells were not labeled by S100β, whereas 20 of the S100β-positive cells were not labeled by Lucifer yellow.

[*] $P < 0.05$.

[**] $P < 0.01$, statistically significantly different dye-labeled cell counts compared to 8% LYVS (ANOVA and Bonferroni test).

[***] $P < 0.001$ octanol-treated vs. untreated cells injected with 4% LYVS + 4% LYCH (*t*-test).